Post-Print

S. Ceccherini, K.V. Mani, F. Topputo
Combined System-Trajectory Design for Geostationary Orbit Platforms on Hybrid Transfer
Journal of Spacecraft and Rockets, In press - Published online 11/10/2021
doi:10.2514/1.A35012

Combined System–Trajectory Design for Geostationary Orbit Platforms on Hybrid Transfer

Simone Ceccherini*, Karthik V. Mani† and Francesco Topputo‡
Politecnico di Milano, 20156 Milan, Italy

A novel methodology for a combined systems–trajectory optimization for geostationary equatorial orbit (GEO) platform is proposed to obtain comprehensive design solutions. Combined chemical–electric propulsion system is utilized to execute hybrid high-thrust–low-thrust trajectory transfer to GEO, thereby balancing overall system mass and transfer time. A systematic and payload-centric mission design provides a new set of design options to deliver tailored solutions to customized payloads. The hybrid trajectory characterization and spacecraft systems design find the required platform launch mass to deliver a GEO platform with a defined final mass and operational power. Elements of system design are combined with those of multi-spiral low-thrust trajectory optimization as well as radiation absorption and solar array degradation to provide a comprehensive design solution. The result is a wide set of solutions to reach GEO, where fully-chemical and fully-electric transfers represent the boundaries of the hybrid transfer trade space. A payload throughput power of 20 kW entails a spacecraft mass in GEO between 4000 kg and 4550 kg, an initial thrust-to-mass ratio range of $1.7 - 2.3 \times 10^{-4}$ m/s^2, and a coverglass thickness between 4 and 24 mils to guarantee a minimum end-of-life/beginning-of-life power ratio of 85%. In addition, all-electric solutions from different injection orbits yield transfers to GEO with time-of-flight of 60–150 days and an initial mass for the platform, 4400–5500 kg.

*Research Assistant, Department of Aerospace Science and Technology, simone.ceccherini@mail.polimi.it
†Post-Doctoral Fellow, Department of Aerospace Science and Technology, karthikvenkatesh.mani@polimi.it
‡Associate Professor, Department of Aerospace Science and Technology, francesco.topputo@polimi.it, Member AIAA

Nomenclature

d_{cg}	=	coverglass thickness, mils
$D_{\mathrm{p}\rightarrow\mathrm{e}}$	=	proton-to-electron damage ratio
$D\left(E, d_{\mathrm{cg}}\right)$	=	power generation relative damage coefficient
E	=	Energy level for electrons and protons, MeV
$\mathcal{F}, \mathcal{G}$	=	generic functions
g	=	Earth's gravitational acceleration at sea level, m/s^2
I_{sp}	=	specific impulse, s
k_{ep}	=	electric propulsion margin
L_{d}	=	solar array degradation factor during the whole mission lifetime
m	=	spacecraft mass, kg
$\dot{m}$	=	mass-flow rate, kg/s
m_{BT}	=	battery-package mass, kg
m_{IND}	=	trajectory independent subsystems mass, kg
m_{LEO}	=	mass in LEO, kg
m_{SA}	=	solar array mass, kg
m_{SEP}	=	solar electric propulsion system mass, kg
$m_{\mathrm{pl,LV}}$	=	payload mass of launch vehicle upper stage, kg
$m_{\mathrm{s,LV}}$	=	structural mass of launch vehicle upper stage, kg
P	=	power, W
P_{IND}	=	trajectory independent subsystems power, W
$R_{\mathrm{a,so}}$	=	apogee radius of the switching orbit, km
$R_{\mathrm{p,so}}$	=	perigee radius of the switching orbit, km
T	=	thrust, N
t_0	=	initial epoch for low-thrust phase
t_f	=	final epoch for low-thrust phase
V	=	voltage, V
X	=	efficiency of path from solar array/battery-package to loads
ΔV	=	velocity change, m/s
$\boldsymbol{\lambda}_0$	=	initial costates vector for low-thrust transfer
$\mathrm{d}\Phi\left(E\right)/\mathrm{d}E$	=	differential fluence, parts/(cm^2 MeV)
Φ_{1MeVe}	=	equivalent fluence of 1MeV of electrons, parts/cm^2

Ω = right ascension of ascending node

τ = total transfer time, days

μ = Earth's gravitational parameter, km^3/s^2

Subscripts

CM = central meridian

cg = coverglass

cp = chemical propulsion phase

d = daylight

e = electrons

ec = eclipse

ep = electric propulsion phase

jett = jettisoning phase

LV = launch vehicle

p = protons

pl = payload

pr = propellant

EP = electric propulsion system level

TH,single = thruster-level

I. Introduction

Cost saving, in terms of spacecraft mass and operation time, has become one of the key driving parameters for mission design. Until recently, the strategy to deliver a spacecraft in geostationary equatorial orbit (GEO) relied entirely on chemical propulsion (CP). Starting from the injection into geosynchronous transfer orbit (GTO), the ideal transfer time to reach the GEO belt is less than one day by using the standard Hohmann transfer [1]. This solution is fast and simple at system level, but the penalty in terms of launched-to-final mass ratio needs to be considered; which is ~1.5–2 depending on the specific impulse of the CP. In the last decade, the increasing trend in the commercial GEO satellite signal throughput capacity has led to an increase in the number of communication payloads (e.g. antennas, amplifiers etc.) and an increase in power demands up to 20–25 kW, resulting in an increase in power system mass as well as overall spacecraft mass. Therefore, to account for this change, electric propulsion (EP) solutions were conceived for GEO

satellites in order to a) utilize the high power generation capacity during transfer when the payloads are not in use and b) to decrease the propulsion system mass, thereby increasing the allocation for communication payloads, due to the high specific impulse of EP systems.

In 2015, Boeing 702SP satellite platform entered the geostationary Earth orbit equipped only with low-thrust EP system, thus paving the way for all-electric satellites [2]. Two years later, the Airbus Eurostar E3000 EOR version achieved the same goal*. The launched initial-to-final mass ratios of these spacecraft lay between 1.05–1.20, depending on the EP system performance.

Considering the GEO region, the telecommunication spacecraft have the lion's share in the market, which is a very profitable business [3]. Consequently, they are the most attractive platforms to enhance. The monetary benefits may not only be related to the reduction in launched mass, but also to the reduction in the time to commence commercial operations. Thus, system mass and time of flight play a key role in maximizing the benefit.

The standard GTO was first proposed as a starting orbit to reach GEO only using CP systems. Recently, all-electric transfer solutions to GEO were proposed with a higher apogee radius than that of GTO, such as super synchronous transfer orbit (SSTO), and to subsequently pursue low-thrust insertion. Analysing fully-chemical transfer (FCT) and fully-electric transfer (FET), the former leads to a very large system mass while yielding a shorter transfer time while the latter leads to a very long transfer time and a smaller system mass. Additionally, longer transfer times lead to high radiation accumulation and damage. Therefore, a hybrid transfer (HT) that utilizes CP and EP in different mission phases achieves a balance between time-of-flight and mass-at-launch.

The first analysis about the usage of CP and EP was developed in [4]. Successively, in the last 30 years, various works have considered the combination of those propulsion systems. A patching method was proposed in [5] using a package SEPSPOT [6], developed at *Charles Stark Draper Laboratory*. The total velocity cost for high-thrust and low-thrust paths were fixed, and an intermediate switching orbit was determined to minimize the overall transfer cost.

A coplanar transfer from low-Earth orbit (LEO) to GEO that exploits CP with EP paths was investigated in [7]. Effects of the overall radiation dosage were characterized and a preliminary design on the hybrid vehicle was developed at system level. The aim was to reduce the total radiation loads on the spacecraft and to provide reduced total flight times. In [8], an optimization for the specific impulse of the EP system was proposed based on chemical apogee motor's specific impulse. This optimum value was computed for both two-stage and three-stage missions, which includes also the ΔV provided by the launch vehicle. That procedure maximizes the mass delivered in the Geostationary belt region. Then, a comprehensive analysis of GEO insertion with combined chemical and electric propulsion stages was developed in [9]. The forward approach used to characterize the mission, i.e., from the initial orbit to the final orbit, relied on six free design variables and included the effect of eclipses and power degradation as well as launcher performances.

In [10], an algorithm was developed to rapidly perform trade studies for transfers with high-thrust and low-thrust

*ESA role in Europe's first all-electric telecom satellite, retrieved on Mar 2021.

trajectories. The mission was characterized based on a backward strategy, that is from GEO to circular LEO. Accordingly, the initial known parameters were the mass delivered into the final orbit, the desired EP performances, and the low-thrust time of flight. Hybrid transfers have also been investigated to reach Moon [11, 12], NEO [13], and Mars [14, 15].

While the previous works focused separately on high/low-thrust trajectory optimization solutions, on spacecraft system design and on performance degradation analysis due to radiation absorption, this study integrates those narratives and aims to create a novel combined systems–trajectory design solution, including radiation effects, for hybrid LEO to GEO transfers for GEO satellite platforms. It proposes a systematic procedure to describe a new family of hybrid transfer solutions, concomitant with platform design, in pursuance to widen the trade space in designing GEO missions with high-power payload. The system–trajectory design and optimization become payload-centric, i.e., fixing the payload properties and optimizing the system design parameters and mission trajectory, to provide the widest range of options to deliver tailored solutions to the customer. The radiation absorbed is evaluated from the beginning to the end of the mission together with a procedure to customize the coverglass thickness for each solution that is included in the overall platform design. Additionally, the performance of FET to GEO from injection orbits different from the usual ones, i.e., GTO and SSTO, are critically analyzed by including a parametric model of launcher's payload capacity.

This work follows the following procedure to achieve the goal of combined systems–trajectory design: first, the mission analysis of the applied hybrid transfer concept is outlined in Sec. II along with the estimation of launch vehicle (LV)'s payload capacity at launch and the optimization of trajectories for high- and low-thrust phases. The radiation environment is investigated in Sec. III. Here, the radiation sources and models are considered. Moreover, the radiation absorption effects on the solar array are modeled and evaluated. Then, the spacecraft's subsystem modelling is described in Sec. IV, where the importance is placed on the payload mass and power budget, the design of both propulsion systems, chemical and electric, and the power generation system. The proposed methodology to assess the HT mission is delineated in Sec. V, where the combination among trajectory optimization, systems design and optimization, radiation absorption effects and mission design choices is outlined. Finally, the results of that methodology is reported in Sec. VI, where a critical analysis is performed by computing key parameters of spacecraft systems and transfer to GEO, by evaluating the HT mission performance sensitivity to payload variations, and by characterizing and comparing all-electric GEO platform with respect to non-traditional injection orbits. Overall, this work presents a comprehensive characterization of the combined-systems trajectory design such that a wide range of solutions for GEO platform on hybrid transfers are obtained.

II. Mission analysis

A. Hybrid Transfer concept

The mission profile follows a path that exploits the advantages of the two types of propulsion. The Oberth Effect [16] dictates that maneuvering is more suitable where the orbital velocity is higher, because the cost of ΔV has a nonlinear effect on the vehicle's kinetic energy. Thus, the use of chemical propulsion (CP) is more efficient than the electric propulsion (EP) in the first steps of the trajectory, i.e., close to the primary body. This is why throughout the stated analysis, as well as in most of the literature [8–10], a high-thrust path is followed by a low-thrust phase. In order to achieve a higher thrust-to-mass ratio for EP phase, the hybrid platform is made of two units at conceptual level, thus giving rise to the dual-stage configuration, as depicted in Fig. 1. Here, the dashed-trapezoidal block symbolizes the chemical propulsion module (CPM) and the small-rectangle one represents the EP system. Planning the jettisoning phase for the CP system shall follow the guidelines to mitigate the space debris given by [17].

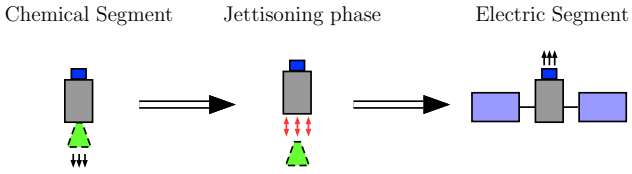

Fig. 1 Proposed dual stage configuration for hybrid transfer.

The mission initiates once the launch vehicle (LV) releases the spacecraft in a low-Earth orbit (LEO) with an inclination of 5° (compatible with Kourou launch-site). One of the most expensive maneuvers in terms of ΔV is orbital plane change maneuver, mainly if it is combined with a spacecraft velocity change maneuver [18]. Therefore, a coplanar orbital change maneuver is accomplished by CP and it is executed by means of two burns. Thus, the hybrid transfer (HT) platform reaches an intermediate orbit along which the CPM shall be jettisoned. The EP trajectory commences once this is accomplished. The intermediate orbit is called switching orbit and the grid considered for its parameterization in terms of perigee and apogee radii is illustrated in Fig. 2. Specifically, each switching orbit proposed represents the starting orbit of the low-thrust transfer to geostationary equatorial orbit (GEO). This also allows for an analysis of the fully-chemical transfer (FCT) and the fully-electric transfer (FET) as special cases of the proposed search space, since they occur when the switching orbits coincide with GEO and LEO, respectively. It should be noted that when the fully high-thrust transfer to GEO is analyzed, the CP performs also the required plane change by bi-impulsive fuel-optimal maneuvers, according to the procedure in [18].

In this work, the set of HT to GEO is characterized following a top-down or backward track approach, i.e., from GEO to LEO. In this way, a payload-centric mission design is pursued. However, the computational time to retrieve the whole solution-space is high since several properties of the platform at the end of the trajectory are dependent on transfer itself, as shown later in this paper.

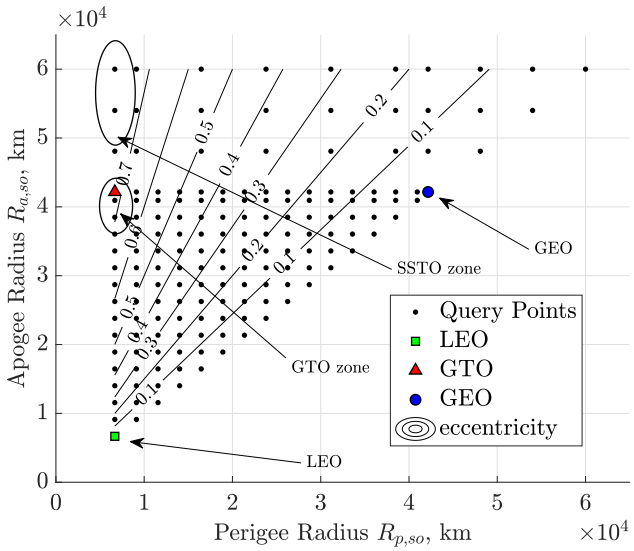

Fig. 2 Search space for switching orbits.

B. Low-thrust transfer phase

Searching for optimal low-thrust transfers to GEO from several injection orbits with high eccentricity (0.6–0.7, see Fig. 2) is one of the major challenges of the orbit-path analysis. EP systems have high specific impulses which makes them highly suitable for executing low-thrust transfers. Furthermore, the usage of EP offers to exploit several values of thrust and specific impulse by varying the signal voltage and power at propulsion system level, based on the mission requirements. However, the electric thruster performance is constrained within an operative envelope, which subsequently constrains the trajectory optimization. Trajectory optimization minimizes either the transfer time (time-optimal) or the propellant consumption (fuel-optimal). Time-optimal solutions have continuous thrusting while fuel-optimal solutions have intermittent thruster operation also known as bang-bang control. In this work, time-optimal solution is pursued. The optimization scheme is solved using a combination of indirect, multi-homotopy methods (on thrust and orbital parameters continuation) and single & multiple shooting scheme through the Low-Thrust Trajectory Optimization (LT2O) code [19], developed at Politecnico di Milano. The aforementioned approach is used to solve the two point boundary value problem (TPBVP) in the controlled two-body model expressed in Modified Equinoctial Elements (MEE) [20].

Time-optimal solution requires continuous thruster operation, even during eclipses. Among the key features of the introduced system-trajectory design, the battery package is sized accordingly to feed the EP system with the required power to ensure an always-on thruster condition. Thus, the transfer time is unaffected by eclipses. Generally, GEO platforms are equipped with a substantial battery capacity to handle nominal operations even during eclipses. The design choice for battery sizing copes with time optimal transfer since, when TPBVP is considered the throttling factor for EP thrust is equal to 1 for the whole EP trajectory τ_{ep} [19, 21]. This choice is further explained in Sec. IV.C. The

power delivery requirements are analyzed for real eclipses duration, which are in turn calculated based on the departure epoch. The rationale behind the battery sizing design choice is to allow the spacecraft to operate without any power loss during the mission. During the transfer, the thruster input power is considered constant. Furthermore, dealing with TPBVP perturbations, the throttling factor for EP thrust is equal to 1 for the whole low-thrust duration, τ_{ep} [19, 21]. Additionally, possible small-scale thrust-outages are neglected. The time-optimal solution also expedites the time to commence the service of commercial GEO spacecraft and this has a significant economic impact [22].

1. Spacecraft mass analysis for electric orbit raising

The mass-flow rate for the EP system is expressed using,

$$\dot{m}_{ep} = n_{\mathrm{TH,single}} \, \frac{2\,\eta\,\mathrm{P}}{\left(\mathrm{g}\,\mathrm{I}_{\mathrm{sp,ep}}\right)^2} \tag{1}$$

where $n_{\mathrm{TH,single}}$ is the number of operating EP thrusters, P is the thruster input power, η is the thruster total efficiency, g is the gravitational acceleration at sea level (equal to 9.8063 m/s^2) and $\mathrm{I_{sp}}$ is the specific impulse. It is assumed that if two or more EP engine propel the platform at the same time, they will operate at the same working-point, e.g., thrust and specific impulse. This is to cancel any residual torque. Since the right-hand side in Eq. (1) is constant during the transfer, $\dot{m}_{ep}$ could easily be integrated. Let t_0 and t_f be the starting and ending epochs for low-thrust portion, respectively, such as $\tau_{\mathrm{ep}} = t_{\mathrm{f}} - t_0$. The satellite mass values at these epochs are

$$m_{ep}\,(t_0) = m_A + m_B\;\tau_{ep}\dot{m}_{ep} \tag{2}$$

$$m_{ep}\,(t_f) = m_A + (m_B - 1)\;\tau_{ep}\dot{m}_{ep} \tag{3}$$

where m_A (kg) and m_B (-) are mass and a mass-related parameters, respectively, that are expressed based on: 1) the known payload and bus masses, m_{PL} (defined later in Eq. (26)) and m_{BUS} (defined later in Eq. (27)) respectively, 2) the propellant spent for the end of life (EOL) disposal maneuver, $m_{\mathrm{pr,EOL}}$, 3) the estimated propellant spent $m_{\mathrm{pr,inGEO}}$ for secondary maneuver ΔV_{inGEO}, and 4) the EP margin, $\mathrm{k_{ep}}$, that takes into account the EP tankage fraction, which has been assumed 0.1 after the analysis of data in [23], and an EP propellant margin of 5%.

The spacecraft mass relations for the low-thrust transfer phase at its commencement and ending are:

$$m_{ep}\,(t_0) = m_{\mathrm{PL}} + m_{\mathrm{BUS}} + \left(\tau_{ep}\dot{m}_{\mathrm{ep}} + m_{\mathrm{pr,inGEO}} + m_{\mathrm{pr,EOL}}\right)\left(1 + k_{\mathrm{ep}}\right) \tag{4}$$

$$m_{ep}\,(t_{\mathrm{f}}) = m_{\mathrm{PL}} + m_{\mathrm{BUS}} + \left(\tau_{ep}\dot{m}_{\mathrm{ep}} + m_{\mathrm{pr,inGEO}} + m_{\mathrm{pr,EOL}}\right) k_{\mathrm{ep}} + m_{\mathrm{pr,inGEO}} + m_{\mathrm{pr,EOL}} \tag{5}$$

In Eq. (5), it can be observed that the propellant consumption for the low-thrust transfer, $\tau_{ep}\dot{m}_{ep}$ is subtracted from Eq. (4).

The spacecraft mass at the planned EOL phase is expressed as,

$$m_{\mathrm{GEO}}\left(t_{\mathrm{EOL}}\right) = m_{\mathrm{PL}} + m_{\mathrm{BUS}} + \left(\tau_{ep}\dot{m}_{\mathrm{ep}} + m_{\mathrm{pr,inGEO}} + m_{\mathrm{p,EOL}}\right) k_{\mathrm{ep}} + m_{\mathrm{pr,EOL}} \tag{6}$$

where $m_{GEO}\left(t_{EOL}\right)$ is the platform mass at the epoch when the EOL maneuver happens. The propellant mass at EOL $m_{\mathrm{p,EOL}}$ is obtained by combining the EP mass-flow rate (Eq. (1)) and the estimated transfer time, τ_{disp}, to reach a Graveyard orbit with altitude of 310 km above GEO. This value is obtained following guidelines in [17], with assumed solar radiation pressure coefficient of 1.5 kg/m^2 and an aspect area over dry mass of 0.05 m^2/kg. Whereas, the disposal trajectory from GEO to the Graveyard orbit region is time-optimized for a worst case initial control authority of $T/m = 1 \times 10^{-4}$ m/s^2 and for specific impulses in a range from 1500 to 3000 s. Since the obtained results are in a very narrow transfer time region, τ_{disp} was fixed to 1.58 days as wort-case scenario, regardless of the specific impulse among the investigated ones. The propellant required for orbit and attitude maintenance in GEO is obtained using the rocket equation for Eqs. (5) and (6), which is then expressed as

$$m_{\mathrm{pr,inGEO}} = m_{ep}\left(t_f\right)\left(1 - e^{-Z}\right), \tag{7}$$

where Z is equal to $\Delta V_{\mathrm{inGEO}}/\left(\mathrm{g}\,\mathrm{I}_{\mathrm{sp,ep}}\right)$. In Eq. (7), the ΔV_{inGEO} is computed by summing up the value retrieved in [24] of 80 m/s per year for station keeping (SK) and a yearly assumed value of 50 m/s for attitude control. These ΔV are multiplied by the designed operative lifetime of the payload, called LF from now on. Then, by using Eqs. (4) to (7), the explicit expressions for m_A and m_B are

$$m_A = \left[m_{\mathrm{PL}} + m_{\mathrm{BUS}} + m_{\mathrm{p,EOL}}\left(1 + k_{\mathrm{ep}}\right)\right]\left[1 + \frac{\left(1 + k_{\mathrm{ep}}\right)\left(1 - e^{-Z}\right)}{e^{-Z}\left(1 + k_{\mathrm{ep}}\right) - k_{\mathrm{ep}}}\right] \tag{8}$$

$$m_B = \left(1 + k_{\mathrm{ep}}\right)\left[1 + \frac{k_{\mathrm{ep}}\left(1 - e^{-Z}\right)}{e^{-Z}\left(1 + k_{\mathrm{ep}}\right) - k_{\mathrm{ep}}}\right] \tag{9}$$

2. Trajectory computation

Payload power is a key driving parameter for the initial design of the spacecraft platform, elaborated in Sec. IV. The thruster input power and consequently, the EP system performance, i.e., thrust and specific impulse values, are calculated based on the initial platform design. Utilizing these EP system performance values, time-optimal solutions for each orbit within the search space (Fig. 2) have to be obtained.

As mentioned before, the orbital dynamics is formulated using MEE. If compared to Cartesian coordinates, MEE guarantee good numerical stability when dealing with multi-spiral low-thrust transfers [25]. Moreover, when MEE are used, the boundary conditions of orbit-to-orbit transfers are expressed as fixed values for some elements of the initial

and final states, rather than nonlinear functions of them. In addition, by considering the space vehicle mass dynamics to the orbital one, the well known augmented system of equations of motion is obtained [19, 21]. For the sake of clarity, let the augmented state vector be $\boldsymbol{x} = \left[p, e_x, e_y, h_x, h_y, L, m\right]^\top$, where the first six components are the MEE and m is the generic satellite mass. Then, $\boldsymbol{\lambda} = \left[\boldsymbol{\lambda}_{\text{mee}}^\top, \lambda_m\right]^\top$ is the vector of costates, with $\boldsymbol{\lambda}_{\text{mee}} = \left[\lambda_p, \lambda_{e_x}, \lambda_{e_y}, \lambda_{h_x}, \lambda_{h_y}, \lambda_L\right]^\top$. Consequently to the system of equations represented by state $\boldsymbol{x}$ and costate $\boldsymbol{\lambda}$ dynamics, convergence issues should be taken into account [19].

The problem is highly sensitive to the initial guesses, i.e., initial costates vector at time t_0 and EP time of flight. In order to decrease the computational time, a database of TPBVP for the considered switching orbit is built with a control authority range of $10^{-4} - 10^{-3}$ m/s^2, and three specific impulses values that are 1500 s, 2000 s, and 2500 s. The boundary conditions used are the ones listed in Table 1, where classical orbital elements are used to ease their physical representation. The LT2O code is robust and can obtain time optimal transfers to GEO given an arbitrary starting orb1it [19].

Table 1 Boundary conditions to build the low-thrust transfers database.

	a [km]	e [−]	i [deg]	Ω [deg]	ω [deg]	θ [deg]	Mass [kg]
Initial Orbit	$\frac{R_{\text{a,so}}+R_{\text{p,so}}}{2}$	$\frac{R_{\text{p,so}}-R_{\text{a,so}}}{R_{\text{a,so}}+R_{\text{p,so}}}$	5	0	0	π	1000
Final Orbit	R_{GEO}	0	0	FREE	FREE	FREE	FREE

The quantities $R_{\text{a,so}}$ and $R_{\text{p,so}}$ are apogee and perigee radius of the switching orbit. Those time-optimal solutions serve as guess generator of initial costates vector and EP transfer time. For each j-th switching orbit defined in Fig. 2, based on acceleration given by EP and specific impulse, a set of least-square curve-fitting functions are obtained to guess the initial costates vector ($\boldsymbol{\lambda}_0$) in Eq. (10), where the augmented state of the dynamics represents the six MEE component and spacecraft mass-time history.

$$\boldsymbol{\lambda}_{0,i} = \mathcal{F}_i \left(\frac{T}{\text{m}_0},\ I_{\text{sp}}\right); \quad i = 1, ..., 7; \quad \text{each j-th switching orbit} \tag{10}$$

In Eq. (10), $\mathcal{F}_i$ is a transformation from $\mathbb{R}^2$ to $\mathbb{R}^7$. Then, for each j-th switching orbit, a surface is obtained through a nonlinear least square fitting process for guessing the transfer duration (τ_{ep}), given T and $I_{\text{sp,ep}}$ (see [19] for more details). In [26], an exponential behavior is suggested for the 3D function under investigation, yielding

$$\tau_{ep} = a_i \left(\frac{T}{m_0}\right)^{b_i} \left(I_{\text{sp}}\right)^{c_i} + d_i \left(\frac{T}{m_0}\right)^{e_i}; \quad \text{each j-th switching orbit} \tag{11}$$

To solve the TPBVP, an analysis of the boundary conditions is done first. Except for the spacecraft mass at epoch t_0, unknown at this stage because of the top-down (or backward) approach, and the initial Right Ascension of Ascending

Node (RAAN), Ω_i, which depends on launcher ascent dynamics and launch epoch, the boundary conditions are the same as those used in Table 1 for building the initial guess generator. The value for Ω_i is computed using

$$\Omega_i = \Omega_{\text{CM}} + 182 \text{ deg} \tag{12}$$

with Ω_{CM} the argument of the central meridian (Greenwich Meridian) at the departure epoch [12]. The RAAN profile in Eq. (12) refers to a standard commercial geosynchronous transfer orbit (GTO) with Ariane 5 ECA from Kourou, French Guyana, and it is assumed to be valid for the LV investigated in this paper. In accordance to Eq. (12), Table 1, and the trend of standard launch windows at first perigee passage for Ariane 5 [27], the departure epoch February 23, 2020 - 22:50:00.00 is selected to get Ω_i as close to zero as possible. This way allows to support the convergence of TPBVP and to decrease the computational time to obtain the solutions in Sec. VI.

Initializing the available thrust and specific impulse for electric orbit raising (EOR) from the EP system design (details in Sec. IV.B), the missing quantities to initialize the TPBVP are the guessed transfer time and the initial mass of the spacecraft for EP segment. The goal is to find $\boldsymbol{\lambda}_0$ and the initial thrust-to-mass ratio such that the solution of TPBVP adheres to the spacecraft mass model expressed through Eqs. (2), (3) and (6) . By combining Eqs. (2), (8) and (9) with the estimated EP transfer time in Eq. (11), the initial guesses for the control authority and EP transfer time are computed. Thus, the trajectory optimization problem is well posed.

In pursuit to decrease the computational time needed to complete the characterization of EP phase, the procedure described in the workflow 1 is used to analyze path from each switching orbit to GEO.

C. High-thrust transfer Phase

Fuel-optimal strategy is chosen for bi-impulsive, planar maneuver that starts in LEO and ends at the switching orbit. The cost (ΔV_{cp}) and the duration (τ_{cp}) of each CP maneuver are expressed using Eqs. (13) and (14). It is assumed that the spacecraft is maneuvered at perigee and apogee.

$$\Delta V_{\text{cp}} = \mathcal{F}\left(R_{\text{p,so}},\ R_{\text{a,so}}\right) \tag{13}$$

$$\tau_{\text{cp,transfer}} = \mathcal{G}\left(R_{\text{p,so}},\ R_{\text{a,so}}\right) \tag{14}$$

The detachment of CPM from the main platform is crucial in designing HT to GEO. While there is a gain in terms of thrust-to-mass ratio, there is a penalty in terms of CP system complexity. The CPM should re-enter in the Earth atmosphere or be disposed in a safe orbit following guidelines in [17]. Disposal orbits are forbidden within LEO zone (up to an altitude of 2200 km), navigation satellites region (altitude from 19000 to 24000 km), and the GEO zone (± 200 km from GEO altitude). Monte Carlo simulations of end-of-life orbital propagation for several orbits are performed

Workflow 1: Low-thrust trajectory computation strategy.

Input: I_{sp} and T by the EP system design; initial T/m for low-thrust phase and guessed EP transfer time by combining Eq. (2) with Eq. (11). Then, guessed initial costates vector invoking Eq. (10);

Solving TPBVP: first attempt with single shooting. Then, if Low-Thrust Trajectory Optimisation (LT2O) does not converge, multiple shooting method is used;

if *LT2O converges* **then**

  Analyze the violation of spacecraft mass model constraint in Eq. (2);

  if $\|\Delta\left(T/m\Big|_{t_0}\right)\| \leq 2.0\times10^{-6}$ m/s^2*, which is supposed 2 order of magnitude lower than the expected one* **then**

    Mission design continues

  else

    Start again the workflow with the latest input values;

  end

else

  Forward integration by exploiting the last quasi-optimal solution of TPBVP to get the EP trajectory; then, analyze the outcome critically with respect to errors for final boundary conditions for position, velocity, and inclination;

  if *Obtained solutions are quasi-optimal* **then**

    Mission design continues

  else

    Increase the maximum iteration of LT2O or discard the results

  end

  ;

end

Output: Time-history for state, co-states, thrust direction, and eclipse periods.

using the tool STELA developed by CNES [28]. Various properties for the CPM are assumed for the worst case scenario and a uniform distribution of six months time period has been added to the departure epoch defined in Sec. II.B to set the epoch for the simulations. In order to do a preliminary estimation of the required ΔV for safe re-entry or disposal maneuvers, the function in Eq. (15) is used.

$$\Delta V_{\text{debris}} = \mathcal{F}\left(R_{\text{p,so}}\ R_{\text{a,so}}\right) \tag{15}$$

This is based on the perigee and apogee radii of the switching orbit, i.e., where the jettisoning phase happens. The resulting map is shown in Fig. 3.

Regardless of the debris mitigation strategy, the module shall be passivated to eliminate the stored energy on the spacecraft stage to reduce the chance of disintegration. The detachment of CPM should take place in maximum one orbital period referred to the switching orbit, $\tau_{\text{jett}} = 2\pi\left(\left(\frac{R_{\text{p,so}}+R_{\text{a,so}}}{2}\right)^3/\mu\right)^{1/2}$ with $\mu = 398600.4354$ km^3/s^2. Thus, the overall time accounted for the CP phase, τ_{cp}, is

$$\tau_{\text{cp}} = \tau_{\text{cp,transfer}} + \tau_{\text{jett}} \tag{16}$$

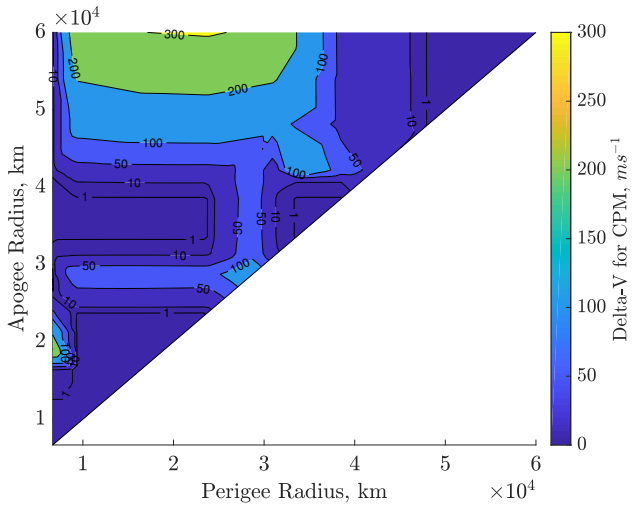

Fig. 3 Cost map accounted for debris mitigation strategy, referring to Eq. (15).

D. Launch-vehicle payload capability

A simplified model of Ariane 64 payload capability for 6 deg inclination injection orbits has been derived through the following steps, in order to perform a parametric analysis on non-standard injection orbit for FET to GEO. It is assumed that Eq. (12) is valid also for Ariane 64.

1) The mass capability of the launcher is computed for a fixed perigee altitude of 250 km and the desired apogee altitude $R_{\mathrm{a,so}}$ through

$$\hat{m} = \mathcal{G}\left(h_{\mathrm{a}}\right), \tag{17}$$

where $\mathcal{G}$ is the best curve to fit Ariane 5 ECA payload capacity versus apogee injection data [27]. Then, it is adapted for Ariane 64 GTO payload capability [29].

2) It is assumed that the payload mass is delivered with a single impulsive apogee maneuver, if needed, to achieve $R_{\mathrm{p,so}}$. That maneuver takes into account the structural mass of the upper stage of the launcher, $m_{s,LV}$, and the specific impulse of the Vinci engine ($I_{\mathrm{sp,LV}}$) [29]. No gravity losses have been considered. The delivered payload mass is then expressed using,

$$m_{\mathrm{pl,LV}} = \mathcal{M}\left(R_{pedp,so}, \hat{m}(h_a), m_{\mathrm{s,LV}}, I_{sp,LV}\right). \tag{18}$$

In Eq. (18) the function $\mathcal{M}$ represents the rocket equation used to study the maneuver to achieve the desired injection orbit, i.e., desired switching orbit from the orbit characterized by $h_p = 250$ km and variable h_a. The maximum payload capability is computed for a representative set of orbits with perigee radius between 8,500 and 21,000 km and apogee between 20,500 and 41,500 km. In addition, the payload capability for the starting orbit previously defined is assumed to be of a LEO with inclination greater than the required one, and that value is

21,000 kg,

III. Environment Analysis

Analysis of the radiation environment is fundamental for designing both manned and unmanned mission. The present study focuses on a region from low-Earth orbit (LEO) to the geostationary equatorial orbit (GEO) belt region. Thus, the radiation source affecting solar arrays are the trapped particles inside the Van Allen belt, i.e., protons and electrons, and the Solar Proton Events (SPE). Single Event failures are considered out-of-scope in this work and therefore the effects of Galactic Cosmic Rays are neglected.

A. Radiation Models

The energy spectra for the trapped radiation environment models is evaluated using the AE9/AP9 software package described in [30]. Table 2 lists the radiations sources considered during each phase of the mission. Radiation absorption during high-thrust segment is not considered because the chemical propulsion (CP) total time of flight in Eq. (16) is very low compared to the electric propulsion (EP) transfer and the usual operative lifetime in GEO. Additionally, SPE can be neglected during the low-thrust transfer for mission in GEO [31]. SPE contribution is generated by Space Environment Information System (SPENVIS) software [32], and the Emission of Solar Protons model developed by [33] is adopted.

Table 2 Summary of the radiation source considered during the mission lifetime.

Phases	Protons and Electrons (trapped particles)	Solar Protons Events
High-thrust segment	NO	NO
Low-thrust segment	YES	NO
In GEO operations	YES	YES

The considered trapped electrons and protons energies are in the range of 0.04-8 MeV and 0.1-250 MeV, respectively. The plasma of proton and electron have negligible impact on the solar cell degradation and are therefore not considered in this work.

Since the fluctuation of those particles is not deterministic, the statistical approach generated through the Perturbed Mode with 95^{th} percentile (40 simulations) is used along with the determined EP trajectory data as input. In pursuit to decrease the computational time and to account for the inaccuracies emerging during the forward integration of the low-thrust phase, the absorbed trapped radiation in GEO has been computed offline by running AE9/AP9 model with Perturbed Mode (40 simulations), 95^{th} percentile. The initial epoch in GEO is assumed to be January 01, 2021, which is also the assumed the worst-case threshold for the final epoch of the whole set of EP transfers.

Let the generic differential fluence of a particle be the time integral of the differential flux $\phi(E, r(t), t)$, as expressed

in Eq. (19),

$$\frac{\mathrm{d}\Phi\,(\mathrm{E})}{\mathrm{dE}} = \frac{\mathrm{d}}{\mathrm{dE}} \int \phi\,(E, r\,(t), t)\,dt \tag{19}$$

Here, $r(t)$ is the position vector (trajectory). The trapped particle contribution is computed by applying Eq. (19) for the low-thrust trajectory. The low-thrust trajectory is the result of the transfer optimization process. For the GEO operation leg, an a-priori computation of the trapped particle contribution is performed. In this way, the estimation of the absorbed differential fluences during the overall mission lifetime can be obtained as a function of the particle energy for trapped electrons and protons using Eq. (20)

$$\frac{\mathrm{d}\Phi_{\mathrm{e}}\,(\mathrm{E})}{\mathrm{dE}} = \mathcal{F}\,(\mathrm{E})\Big|_{ep+GEO} \qquad \frac{\mathrm{d}\Phi_{\mathrm{p}}\,(\mathrm{E})}{\mathrm{dE}} = G\,(\mathrm{E})\Big|_{\mathrm{ep+GEO}} \tag{20}$$

The SPE simulation by SPENVIS is run for long term particles, EPS-PSYCHIC (total fluence) with an energy range of 0.1-500 MeVand 95% confidence level. Interpolating those results gives the function in Eq. (21), which represents the estimate differential fluence absorbed for the operative payload time.

$$\frac{\mathrm{d}\Phi_{p,SPE}\,(E)}{\mathrm{d}E} = \mathcal{F}\,\,(E)\Big|_{\mathrm{GEO}} \tag{21}$$

B. Radiation effects

Effects of radiation on the power generation degradation of the solar cells are investigated in this section. The spacecraft utilizes XTJ Solar Cells by Spectrolab [34]. The dependence of solar power generation on temperature variation as well as the absorbed dose vs aluminium thickness are not studied in this paper. The quantities under consideration for the analysis of radiation effects on power generation are the energy of particles, the exposure time span, and the thickness of coverglass. Solar cell degradation is predicted using the equivalent fluence theory developed by NASA JPL, and described in [35–37]. The solar cell degradation L_{d} is computed as the ratio between the actual power generated and the beginning of life (BOL) power, and it is evaluated using

$$L_{\mathrm{d}}(\Phi_{1\mathrm{MeV}}) = 1 - \left[A\ log_{10}\left(1 + \frac{\Phi_{1\mathrm{MeV}} - 10^{13}}{B}\right) + C\ log_{10}\left(1 + \frac{\Phi_{1\mathrm{MeV}} - 10^{13}}{D}\right)\right] \mathrm{H}(\Phi_{1\mathrm{MeV}} - 10^{13}) \tag{22}$$

where $\Phi_{1\mathrm{MeV}e}$ is the equivalent fluence of electrons @1 MeV and $H(\cdot)$ the Heaviside step function. Fig. 4 illustrates the normalized maximum power L_d with respect to the equivalent fluence of 1 MeV of electrons. This is built by fitting Eq. (22) to the data in [38] by using the fitting parameters listed in Table 3.

The proton-to-electron damage ratio, $D_{\mathrm{p}\rightarrow\mathrm{e}}$, and the relative damage coefficient (RDC), $D_{e/p}(E, d_{\mathrm{cg}})$ relative to power generation, for electrons/protons referred to power generation capability of the selected solar cell have been retrieved from SPENVIS database. Since SPENVIS returns RDC values for 8 values of coverglass thickness, i.e., 0,1,3,6,12,20,30,

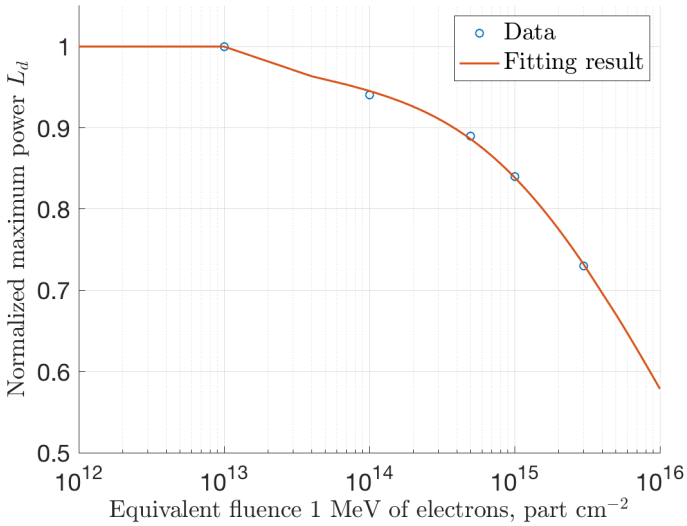

Fig. 4 Curve to estimate the power generation performance of solar cell XTJ by Spectrolab, referring to Eq. (22).

Table 3 Curve-fitting parameters for curve in Eq. (22).

A [−]	B [1MeVe]	C [−]	D [1MeVe]	$\left(R_f^2\right)^\dagger$ [−]
0.02173	10^{12}	0.32120	10^{15}	0.9987

† Coefficient of determination of the curve fitting process.

and 60 mils, the values of $D_{e/p}(E, d_{\text{cg}})$ for a specific coverglass thickness are computed after a curve-fitting, nonlinear least square process on the available data.

The absorbed differential fluences for trapped particles in Eq. (20) are combined with the differential fluence of SPE in Eq. (21), with a given coverglass $\bar{d}_{cg}$, proton-to-electron damage ratio, and the RDC to compute the total equivalent fluence absorbed, $\Phi_{\text{1MeVe,TOT}}$, during the whole mission lifetime, which is expressed using,

$$\Phi_{\text{1MeV}e,e}\ \left(d_{\text{cg}}\right) = \int_{\Delta E_e} \frac{\mathrm{d}\Phi_e\,(E)}{\mathrm{d}E} D_e(E, \bar{d}_{CG})\,\mathrm{d}E \tag{23}$$

$$\Phi_{\text{1MeV}e,p}\ \left(d_{\text{cg}}\right) = D_{\text{p}\to\text{e}}\left(\int_{\Delta E_p} \frac{\mathrm{d}\Phi_p\,(E)}{\mathrm{d}E} D_p(E, \bar{d}_{CG})\,\mathrm{d}E + \int_{\Delta E_{p,SPE}} \frac{\mathrm{d}\Phi_{p,SPE}\,(E)}{\mathrm{d}E} D_p(E, \bar{d}_{CG}) \right) \mathrm{d}E \tag{24}$$

$$\Phi_{\text{1MeVe,TOT}}\ \left(d_{\text{cg}}\right) = \Phi_{\text{1MeV}e,e}\ \left(d_{\text{cg}}\right) + \Phi_{\text{1MeV}e,p}\ \left(d_{\text{cg}}\right) \tag{25}$$

where the ΔE refers to the previously defined energy range within which those integrals are calculated. The total equivalent fluence in Eq. (25) can be computed once the coverglass thickness is given.

IV. Platform System Modeling

Payload-centric design is one of the key features of this work. The goal is to design the spacecraft platform such that any customized payload, with its mass and power requirements, can be delivered at geostationary equatorial orbit (GEO). The payload mass and power are the key parameters that drive the entire platform design. Earth communication satellites are used as baseline in this work and multiple existing GEO payload and platform are analyzed, as listed in Table 4 [39–44]. The platform system modeling to study the family of the proposed mission solutions is formulated in a practical and systematic approach.

A. Payload and Bus Analysis

Table 4 Power and Mass of GEO payload/platform.

Power, W	Mass, kg	Power over Mass, W/kg	Payload/platform
5880	661	8.896	Express AM8 [39]
7000	700	10.000	GMP-TL [40]
7500	500	15.000	702 SP [41]
8000	800	10.000	GeoStar 3 [42]
10000	900	11.111	SmallGEO FLEX [43]
13665	1483	9.214	Express AM7 [39]
22000	2000	11.000	Alphabus [44]

A second-order polynomial law that connects the payload power mass to the generated power is obtained by a curve fitting process to obtain an expression for payload mass as a function of power. The expression obtained is

$$m_{pl} = a_1 P^2 + a_2 P + a_3 \tag{26}$$

with $a_1 = -1.696 \times 10^{-6}$ kg/W^2, $a_2 = 0.1401$ kg/W, and $a_3 = -239.4$ kg. The curve is outlined in Fig. 5.

Concerning the spacecraft bus design, it is assumed that the hybrid transfer (HT) platform is made up of trajectory-independent subsystems, which are detached from the hybrid transfer performances, and trajectory-dependent subsystems that rely on the path followed. Fig. 6 list the subsystems utilized in the design.

The preliminary estimates for mass and power of trajectory-independent subsystems such as attitude and orbital control system, on-board data handling system, telemetry, tracking and command system, and structure of the platform are based on data in [45]. The thermal control system accounts for deployable panel radiator developed for dissipating power to meet the thermal needs of the new generation of high throughput satellites[†]. Trajectory-dependent subsystems are modeled whereas the other ones are lumped as having a cumulative mass, $m_{\text{IND}} = 800 + 10.34 m_{\text{PL}}$ kg, which depends on the payload mass, and a power demand P_{IND} equal to 3400 W. For the sake of safety, a margin of 10% is

[†] `https://artes.esa.int/projects/alphasat-tdp3-2-phase-deployable-radiator`, retrieved on Feb 01 2017.

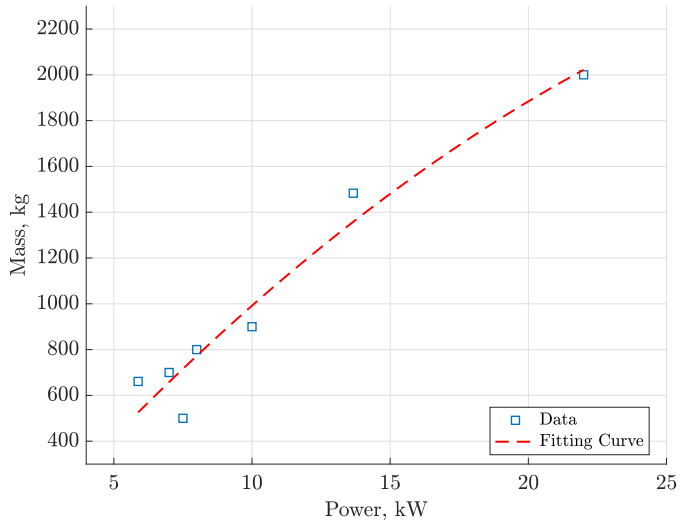

Fig. 5 Curve to estimate mass in power in GEO, referring to Eq. (26).

taken into account for budgets of trajectory-independent subsystems.

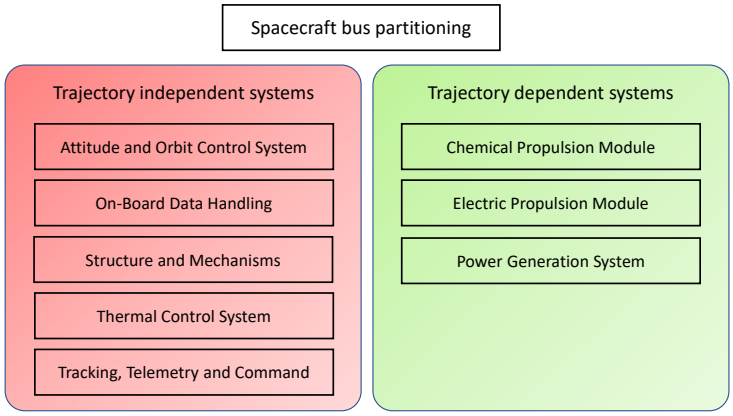

Fig. 6 Spacecraft Bus partitioning.

The preliminary estimates for mass and power of trajectory-independent subsystems such as attitude and orbital control system, on-board data handling system, telemetry, tracking and command system, and structure of the platform are based on data in [45]. The thermal control system accounts for deployable panel radiator developed for dissipating power to meet the thermal needs of the new generation of high throughput satellites[†]. The masses of the trajectory-independent subsystems are lumped and the cumulative mass $m_{\mathrm{IND}} = 800 + 10.34\, m_{\mathrm{PL}}$ kg. The cumulative power consumption of the independent subsystems $P_{\mathrm{IND}} = 3400$ W. For the sake of safety, a margin of 10% is taken into account for budgets.

Trajectory dependent subsystems such as chemical propulsion, electric propulsion, and power generation system are

modeled. The platform bus mass introduced in Sec. II.B.1 is

$$m_{\text{BUS}} = m_{PGS} + m_{\text{SEP}} + m_{\text{IND}} \tag{27}$$

with m_{PGS} and m_{SEP} the mass of the power generation system (PGS) and electric propulsion (EP) system, respectively. Those values are exploded in next sections.

B. Solar Electric Propulsion

The EP system is utilized in primary maneuvers (e.g., orbit raising) and secondary maneuvers (e.g., attitude control) for all the HT scenarios, except for fully-chemical transfer (FCT) where the primary maneuvers are executed only using chemical propulsion (CP). Since the scenarios consider transfer to GEO, the source of energy for the EP system is the solar energy. Thus, from now on, the EP system shall be referred as Solar Electric Propulsion (SEP) system.

The major solar electric propulsion options applicable to GEO platforms are gridded ion tthruster (GIE) and hall-effect thruster (HET). The HET is selected because of the higher thrust-to-power ratio compared to GIE within the considered range of power input in this work [46]. The wide working envelope of those types of electric thrusters guarantees a dual-mode operation , where a HET could operate on high-thrust low-I_{sp} mode for orbit raising and high-I_{sp} low-thrust mode for attitude and orbital control by varying the input power and/or voltage.

The dual-purpose propulsive system described above is one among the several multimode propulsion concepts for orbital transfers that have been investigated in literature, and many others that are currently under investigation. A review of multimode propulsion systems that aims to enhance future spacecraft and space mission is proposed in [47], where hybrid propulsion and multimode space propulsion are analyzed.

For the assessed hybrid transfer in this work, the primary maneuvers could be by way of the HET examined for the analysis are PPS®5000 by Safran and BHT-8000 by Busek. Both of them are fed by Xenon and their properties are described in Table 5.

Table 5 HETs data, retrieved from [48, 49].

Name	Power, kW		Voltage, V		Mass, kg
	P_{min}	P_{max}	V_{min}	V_{max}	
PPS®5000	3.00	6.00	300	800	12
BHT-8000	2.00	8.00	200	400	19.2

Thrust and specific impulse performances of the considered EP thrusters have been obtained from [48, 49] as function of voltage and input power. A polynomial surface fit of the data in [48, 50] using least squares method is done to obtain

have been fitted to using the least square method to obtain polynomial surfaces that are expressed as,

$$T, I_{\text{sp}} = \sum_{i=0}^{N} \sum_{j=0}^{M} \left(p_{i,j}\big|_{T,I_{\text{sp}}} \, \text{V}^i \text{P}^j \right) \tag{28}$$

where the influence of the input voltage and power of the thruster is outlined. Each curve in Eq. (28) is characterized by a set coefficients $p_{i,j}$ and the order of polynomial curves is the maximum between N and M, which are specified in Table 6.

Table 6 Order of fitting, referring to Eq. (28).

	PPS®5000		BHT-8000	
	T	I_{sp}	T	I_{sp}
N	4	5	4	4
M	3	5	3	3

The trend observed in Eq. (28) is that when the input power is constant, a decrease in voltage leads to an increase in thrust, provided other requirements at thruster, e.g., discharge stability and thermal limits, are met. The application of Eq. (28) to the selected electrostatic thrusters produces the surfaces illustrated in Fig. 7.

The power processing unit (PPU) regulates the power and voltage to the thruster. The investigated fully-redundant PPU are listed in Table 7. Those components have a thruster switching capability of 1:2, i.e., one PPU can supply and regulate power to two thrusters, one at a time.

Table 7 Investigated PPU. Data retrieved from [23, 51, 52].

Name	Input	Output				Mass, kg	Efficiency η
	V_{reg}, V	V_{min}, V	V_{max}, V	P_{min}, kW	P_{max}, kW		
MK3	100	100	400	1.5	5	~ 18.6	~ 0.95
New Generation	100	300	400	1.5	20	~ 50[†]	> 0.96

[†] Modular PPU, so the values for P_{max} and the mass are the maximum available.

Since the possibility of having a different EP type thrusters for secondary maneuvers is explored, the BHT-200 by Busek [53] is considered to meet attitude and orbital control system (AOCS) needs. The power required is 200 W, the thrust and specific impulse provided are 13 mN and 1375 s at 250 V, respectively. Operative envelope for BHT-200 has been not considered. Moreover, it is assumed that a customized PPU could be provided by Busek with an input voltage of 100 V, an estimated mass of 5 kg, and electrical efficiency of 1.

SEP system is made up of multiple components such as the HET thruster, external thruster switching unit (ETSU), the filter unit, xenon flow controller, and a propellant management assembly. The ETSU enables the PPUs to increase

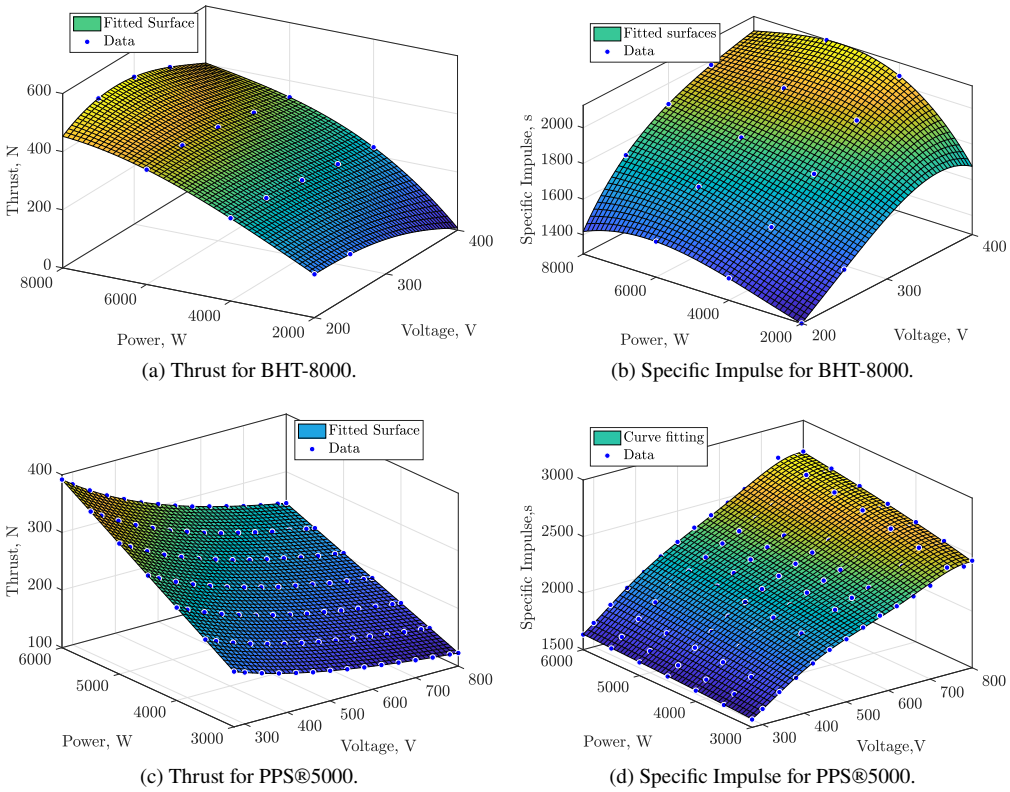

(a) Thrust for BHT-8000.

(b) Specific Impulse for BHT-8000.

(c) Thrust for PPS®5000.

(d) Specific Impulse for PPS®5000.

Fig. 7 Surface to evaluate performance for the selected hall-effect thrusters, referring to Eq. (28).

the thruster switching capability from 1:2 to 2:4. Thus, with the ETSUs, one PPU can handle 4 HETs instead of just 2. Each ETSU has an assumed mass of 4 kg and an efficiency of 1. The filter unit has a mass of 2 kg and counteracts possible electrical perturbations in addition to the selected PPU. Xenon flow controller has a mass of 1.16 kg per thruster and provides the appropriate flow over the range of operating conditions. Propellant management assembly, with a mass of 5 kg [23], enables the regulation of propellant feed pressure. Additionally, a Cold Gas Thruster Assembly that operates using Xenon is considered to counteract failures, as planned in [51] for a GEO platform. Its mass is estimated to be 20 kg and the relative propellant mass is accounted for using the parameter k_{ep} defined in Sec. II.B.1.

The number of thrusters to equip the HT platform is set based on the available power to SEP system, as mentioned in Sec. IV.C. The possible combinations between the selected HETs and PPUs are represented in Fig. 8. The power supply to PPS 5000 is handled by MK3 PPU. A new generation PPU is utilized for BHT 8000. The power supply of the smaller BHT 200 is handled by a Busek PPU customized for that. Practically, architecture 1 represents a single point of failure condition since if PPU fails, the mission cannot be accomplished. However, necessary protective measures have to be taken to prevent this scenario. If the PPU failure is successfully protected against, then Architecture 1 presents a robust option for the low-thrust operations.

Consequently, two architectures are proposed for the SEP system:

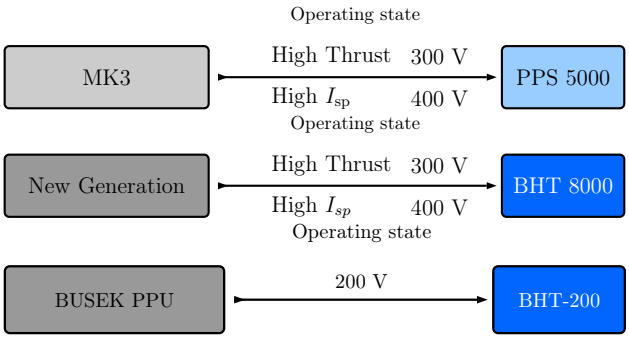

Fig. 8 PPU-HET combinations.

- Architecture 1 in Fig. 9. One nominal thruster, equipped with a gimbal of 10 kg each, performs the orbital raising, whereas, four BHT-200, placed according to EP accommodation of SmallGEO platform by OHB System AG, are in charge of on-orbit maneuvers. Redundancy is taken into account by doubling the thruster from (1 + 4) to (2 + 8).
- Architecture 2 in Fig. 10. Two nominal thrusters perform both the orbit raising and the on-orbit maneuvers. They operate synchronously on two deployment mechanisms, following the robotic arms approach implemented for the platform Eurostar E3000EOR. In order to design a mission to be as safe as possible, the pair of thrusters is doubled, from one per-mechanism to two per-mechanism. As a design choice, the input power to perform control maneuvers is set at 3 kW for both the engines.

The mass budgets (m_{SEP} in Eq. (27)) for the four possible SEP configurations (2 HET, 2 architectures) is listed in Table 8 regardless of the achieved values for thrust and specific impulse. Whereas, for the FCT, 4×2 BHT-200 thrusters are used. Thus, the mass budget for SEP system is 60.54 kg (10% of margin considered). For all selected combinations, the performance of the SEP system can be computed after the available power at thruster-level is known.

Table 8 SEP system mass budget for considered architecture, without the mass of EP tank.

HET model	Architecture 1, kg	Architecture 2, kg
PPS®5000	175.29	214.10
BHT-8000	181.14	245.78

C. Power Generation System

The PGS, also known as Electrical Power System, provides, stores, regulates, and distributes electrical power to the payload and other flight subsystems. Solar array feeds the HT platform during illumination and a battery source is sized to supply energy for electric orbit raising (EOR) and GEO phase operations during eclipses periods. The mass budget of this system (m_{PGS}), at conceptual level, includes the mass of the solar panels and harnsess (m_{SA}), mass of the PGS components ($m_{PGS,CC}$), the mass of batteries (m_{BT}), and the mass of coverglass to shield the solar panel area (m_{CG}).

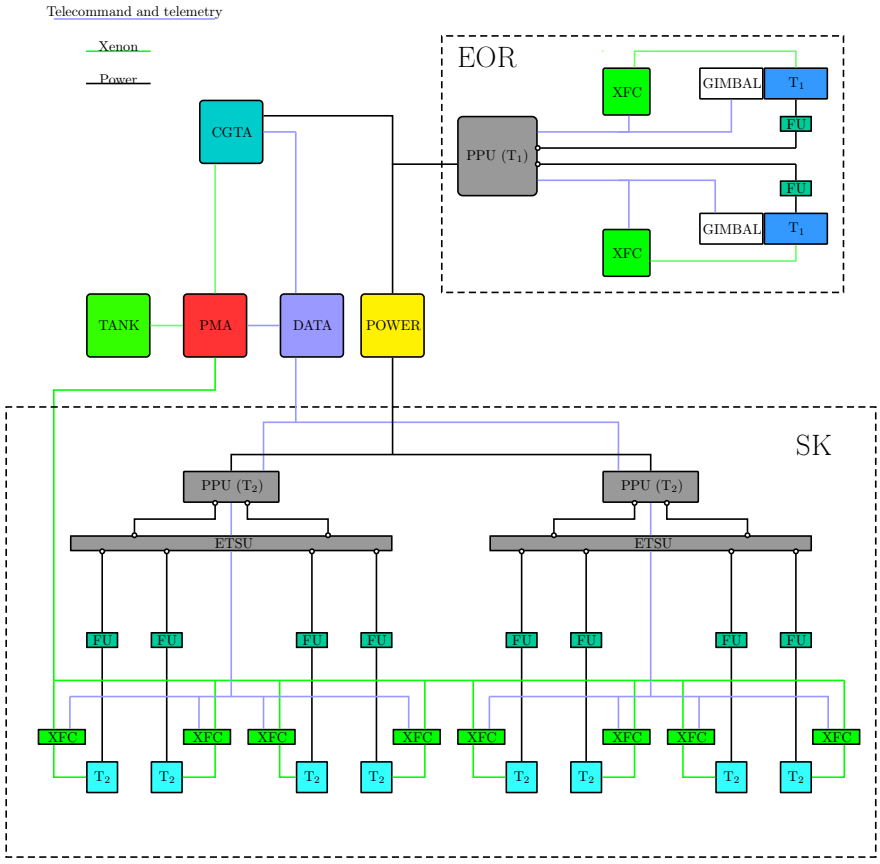

Fig. 9 EP system, architecture 1.

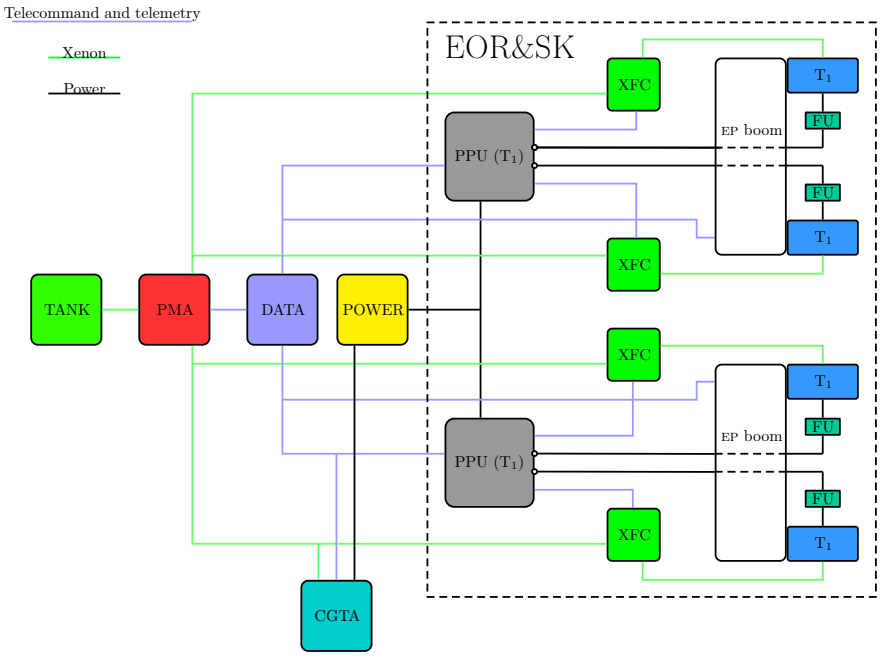

Fig. 10 EP system, architecture 2.

The PSR100V by Airbus Defence and Space [54] is chosen to regulate and distribute power inside the spacecraft. Its power output is 8 to 23 kW, and its mass is computed according to the number of power modules needed (up to 1.5 kW each), within a range of values between 32 kg (for 8kW) and 54 kg (for 23 kW). The rotation around the wing's axis is provided by two solar array drive mechanism, one per wing.

An innovative design is proposed to size the system to deliver the required amount of power at EP thruster level during the low-thrust transfer. The first step is to compute the power that the solar array (P_{SA}) should provide for GEO phase where the payload operates, also during eclipses (T_{ec}) of max 1.21 hour over 22.7 hours of daylight (T_d). The GEO daylight power, P_d, accounts for the power requests of: 1) the payload, 2) the trajectory independent subsystems, 3) the PGS components, e.g., 2 solar array drive mechanism (estimated 50 Wper wing), and 4) SEP system to carry out secondary maneuvers, in configuration 1 or 2. The GEO eclipse power does not account for AOCS operations. The expression for the solar array power is,

$$P_{\mathrm{SA}} = \frac{P_{\mathrm{ec}} T_{\mathrm{ec}}}{X_{\mathrm{ec}} T_{\mathrm{d}}} + \frac{P_{\mathrm{d}}}{X_{\mathrm{d}}} \tag{29}$$

with $X_d = 0.8$ and $X_{ec} = 0.6$ that are typical efficiencies for the delivery of power from solar array/batteries to loads [45]. In addition, the PSR100V performances are taken into account in terms of maximum charging power, current intensity, and output power, which could be increased thanks to the assembled power module.

The total power request during the transfer to GEO could be analyzed for CP and EP phases separately. CP is characterized by a non-rechargeable battery package that feed the spacecraft. As design choice for low-thrust transfer using EP, the power system must provide the same amount of power during daylight and eclipse. The EP phase power request accounts for 1) trajectory independent subsystems, 2) PGS components, and 3) the total available power at thruster level for maneuvering, P_{EP}.

The design philosophy followed here is the minimization of the excess of power generation during GEO operations compared to the entirety of the mission. Two key parameters that drive the power system design are the payload power and the power required from the SEP. To minimize the excess of power and therefore the excess mass of the power generation system, an equal amounts of power shall be spent during GEO operations and the EOR phases. Fig. 11 outlines the concept driving such approach. As outlined in the previous paragraphs, the first task is the computation of the solar array power P_{SA} through Eq. (29) (step 1). Then, the total power should meet the requirement of the power supply regulator (step 2).

The power generated by the solar arrays during GEO phase and the EOR are computed by Eq. (29), and they must be equalized with the aim to satisfy the following relation,

$$P_{SA}\big|_{\mathrm{GEO}} - P_{\mathrm{SA}}(P_{\mathrm{EP}})\big|_{\mathrm{EOR}} = 0 \tag{30}$$

Referring to the solar array power for the EP phase, the unknown quantities are the maximum value of eclipse over

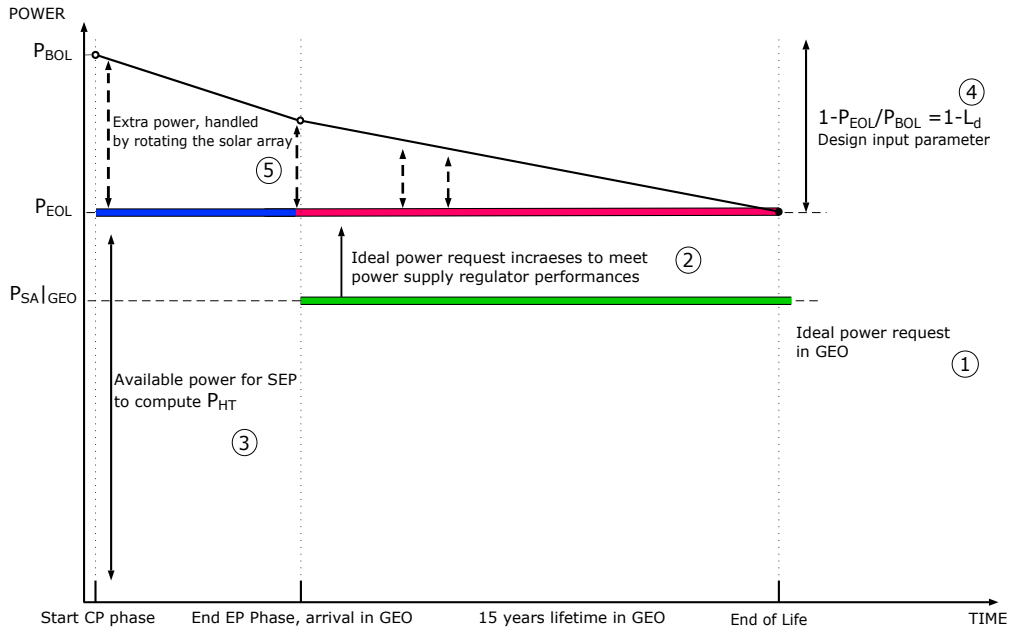

Fig. 11 Approach to set-up the power generated by the solar array during the mission lifetime.

daylight encountered during the transfer and the SEP system power, P_{EP}. This power is adjusted to satisfy Eq. (30) according to the HET constraints in Table 5. Assuming reasonable discrete operating point of the thruster, once the power has been computed, the voltage is kept constant to 300 V to provide the maximum level of thrust available by the function in Eq. (30).

At this stage, the trajectory analysis has not yet been performed. Thus, a first guess on the maximum ratio $T_{\mathrm{ec}}/T_{\mathrm{d}}$ for the EP transfer is established, and it is checked *a posteriori* as explained when battery-package design is described. The first guess used for $T_{\mathrm{ec}}/T_{\mathrm{d}}$ is retrieved from an offline low-Earth orbit (LEO) to GEO low-thrust transfer characterized by an initial thrust-to-mass ratio of 1×10^{-4} m/s^2, specific impulse of 2000 s, and same departure epoch defined in Sec. II.B.2.

Referring to the step 3 in Fig. 11, after $T_{\mathrm{ec}}/T_{\mathrm{d}}$ is fixed, the working envelope of the selected HET allows for the variation of the input power for each EP thruster ($P_{\mathrm{TH,single}}$). In this way, the HT platform system design moves towards optimality. The constraints and guidelines for the procedure are listed in Table 9.

Table 9 Selection of HET operative point

Case	Action
$P_{\mathrm{TH,single}} < P_{\mathrm{HET_{min}}}$	$P_{\mathrm{TH,single}}$ is set to $P_{\mathrm{HET_{min}}}$
$P_{\mathrm{HET_{min}}} \leq P_{\mathrm{TH,single}} \leq P_{\mathrm{HET_{max}}}$	$P_{\mathrm{TH,single}}$ is unchanged
$P_{\mathrm{TH,single}} > P_{\mathrm{HET_{max}}}$	$P_{\mathrm{TH,single}}$ is set to $P_{\mathrm{HET_{max}}}$

Four values of $P_{\mathrm{TH,single}}$ are obtained, one for each SEP configuration (2 HET, 2 architectures) and in turn four

pairs of thrust and specific impulses can be computed using Eq. (28). The SEP configuration is chosen such that the maximum thrust is obtained for primary maneuvers. It should be noted that with a fixed available power at EP engine level, it is not always true that the thrust provided by two thrusters is higher that that of a single thruster since the relationship between input power and thrust is not linear.

The final point for the solar array design is the choice of the degradation factor L_d (step 4), which will define the extra power to be handled by solar array rotating mechanism. Following the concept described above, the power at SEP system could be kept constant during the low-thrust transfer.

It must be noted that the procedure to calculate P_{EP} using Eq. (30) is highly sensitive to the initial guess T_{ec}/T_d relevant for the transfer. Once the thrust and specific impulse have been computed, the low-thrust phase can be characterized. The post-processing of this trajectory leads to three possible scenarios:

1) The obtained value of T_{ec}/T_d is lower than the initial guess. This means that more power can be exploited by SEP for EOR, thus the low-thrust trajectory optimization shall be repeated again starting from the computation of available power at thruster-level. If the input power has been already set to its maximum (third guideline in Table 9), the HT mission design continues.
2) The obtained value of T_{ec}/T_d is greater than the initial guess. The battery-package cannot be fully-charged during at least one eclipse-daylight-eclipse cycle. If the discharge level exceeds a user-defined threshold, the trajectory analysis shall run again with a new guess for T_{ec}/T_d.
3) The obtained value of T_{ec}/T_d is similar to the initial guess, i.e. the ratio between the one computed and the one guessed is between 0.95% and 1.05 %. The HT mission and systems design moves forward.

The Power Generation System sizing concerns also the battery package, which is of great importance since it must supply energy to the SEP system during the eclipses in the electric orbit raising phase. The capacity of the battery package C_{bt} is computed using Eq. (31) [45]:

$$C_{\mathrm{bt}} = \frac{P_{\mathrm{ec}}\, T_{\mathrm{ec}}}{\eta_{\mathrm{bt}}\, N_{\mathrm{bt}}\, DOD}\,, \tag{31}$$

where η_{bt} is the efficiency of cells, N_{bt} is the battery number, and depth of discharge (DOD) represents the percentage of discharge for the battery during one duty cycle.

Li-Ion cells LSE51 made by GS YUASA [55] are considered and it is assumed that the performances of Li-Ion cells do not change if the DOD varies during the mission. Primarily, the batteries are sized to meet the GEO needs in terms of eclipse period and request power with a DOD of 70% and a bus voltage of 96 V as design choice. Similar to the T_{ec}/T_d analysis previously described, the low-thrust trajectory post-processing is fundamental for the battery capacity computation. It shall be verified whether the designed battery meets the EOR requirements in terms of supplied energy and feasibility of a new DOD value for the transfer phase. If the requirements are not met, i.e., battery capacity is not

enough to feed the SEP, one string of cells (Δm_{BT}) is added to the initial battery configuration until the requirements are fulfilled. The EP trajectory entails a maximum DOD of 90%. Consequently, if the Δm_{BT} leads to a difference in magnitude of thrust-to-mass ratio greater than 2.0×10^{-6} m/s^2, the EP trajectory shall be analyzed again with new m_{PGS}.

The area of solar panels is computed based on the standard method in [45] with a bus voltage of 100 V. The geometric packaging efficiency, the angle of loss in GEO, and a fixed ratio between the end of life (EOL) and beginning of life (BOL) power generation, $L_{\mathrm{d,min}}$, are considered in the design of the solar array. Consequently, each HT platform shall not exceed the L_{d} threshold, so giving rise to a different value of coverglass thickness for each switching orbit in Fig. 2. Finally, the masses for the solar array and the coverglass are computed by multiplying the solar panels area with the densities of solar panels and coverglass, 1.76 kg/m^2 and 2550 kg/m^3 respectively. A 10% margin is added for for harnesses.

D. Chemical Propulsion Module

The chemical propulsion module (CPM) consists of engine, tank, valves, and feed lines. Impulsive maneuvers for orbit raising is considered for the CP segment. A bi-propellant system is chosen and it comprises a hypergolic mixture of Monomethylhydrazine (MMH) as fuel and Mixed Oxides of Nitrogen (MON) as oxidizer. The power request for the apogee kick motor (e.g., valves, electronics) is very low, ~50 W, plus a 10% as margin at system level. The nominal performances of the selected thruster are listed in Table 10. The CP system is pressurized by Helium, Composite Overwrapped Pressure Vessels (COPVs) store the fuel, the oxidizer and the pressurant, and their masses are modeled following the procedure in [45].

Table 10 Nominal performances for Liquid apogee kick motor.

	Fuel/Ox	(O/F)	T, N	I_{sp}, s	$\dot{m}$, kg/s	$t_{\mathrm{b.o.}}$, s	Mass, kg
S400-12[†]	MMH/MON	1.65	420	318	0.135	8.3	3.60

[†] From `http://www.space-propulsion.com`

The design of the CPM takes into account the effect of ΔV cost for both the bi-impulse maneuvers, referred to CP segment, and the debris mitigation strategy in Eq. (15). The CPM mass m_{CPM} is calculated using Eq. (32). It should be noted that the initial mass of the low-thrust path ($m_{ep}(t_0)$) influences the propellant spent for CP maneuvers, which in turn affects the CPM mass.

$$m_{\mathrm{CPM}} = \mathcal{F}\left(m_{\mathrm{ep}}\,(t_0),\ \Delta V_{\mathrm{cp}},\ \Delta V_{\mathrm{debris}}, \text{CP tanks and pressurant}\right) \tag{32}$$

V. Methodology

The proposed methodology delineates how the system–trajectory design is optimized with the aim of producing multi-objective solutions. Enhancing the efficiency of hybrid transfer (HT) to geostationary equatorial orbit (GEO) gives rise to a payload-centric platform design. Thus, the mission phases are characterized and analyzed with a top-down (or backward) approach, i.e., from GEO to initial orbit, such that utility of the payload and its characteristics in GEO phase is not compromised.

The key parameter that drives the setting the electric propulsion (EP) working point is the payload power request, as outlined in designing the power generation system (PGS). The *top-down* system–trajectory design logic flow is illustrated in Fig. 12, where some of the key steps are shown. The key challenges lie in solving the low-thrust and high-thrust transfers, and in evaluating the feasibility of mass at launch because it is assessed only at the end of the procedure.

Input parameters payload power, lifetime in GEO, and threshold for ratio between end of life (EOL) over beginning of life (BOL) power generation are utilized in characterizing part of the spacecraft delivered into the Geostationary orbit: the Payload and Bus Analysis (Eq. (26), m_{IND} and P_{IND} in Sec. IV.A), Power Generation System Design (Sec. IV.C), and Solar Electric Propulsion system design (Sec. IV.B). At this point, the Solar Electric Propulsion (SEP) architecture is selected and consequently the working point for the low-thrust phase is selected in terms of Power, Thrust, and Specific Impulse as explained into Sec. IV.C and Sec. II.B, respectively.

The next step is sizing the thickness of coverglass, which is calculated by evaluating the maximum equivalent fluence (Φ_{max}) by Eq. (22) with input threshold degradation factor $L_{\mathrm{d,min}}$. The minimum coverglass thickness required during the payload's in-orbit operative life, $d_{cg,min}$, can be computed by the inverse of Eq. (25) and then used as the first guess value.

Once the the switching orbit is selected among the ones proposed into Fig. 2, the EP segment is analyzed using Work-flow 1 (see Sec. II.B.2). The guess quantities are initialized and the trajectory analysis is set up. The low-thrust trajectory analysis is performed to characterize the appropriate T_{ec}/T_d and feasible depth of discharge (DOD) values during the transfer as already explained in Sec. IV.C (in the flow-chart, it is represented by first elliptic block in Fig. 12).

The total equivalent fluence is evaluated according to the radiation sources considered in different mission segments as listed in Table 2, and the solar array degradation is calculated using Eq. (22). Each trajectory to GEO entails a different distribution of $\Phi_{1\mathrm{MeV}e}$ as function of d_{cg} (see Eq. (25)). If the threshold degradation factor $L_{\mathrm{d,min}}$ exceeds L_{d}, i.e., $L_{\mathrm{d,min}} > L_{\mathrm{d}}$, the required cover glass thickness d_{cg} is increased up to 1.1 times the coverglass thickness needed to match Φ_{max} for the considered HT path. The coverglass thickness increment of 10% causes a minor oversizing of the mass at system-level. However, this is deemed acceptable since it is much lower than the usual mass of a GEO communication platform, e.g., 3000-6000 kg, as the parametric analysis shows in Fig. 13.

Finally the analysis of the chemical propulsion (CP) segment is performed. The dry mass of the chemical propulsion module (CPM) is obtained through Eq. (32). The CP propellant is computed through the combination of Eq. (13), the

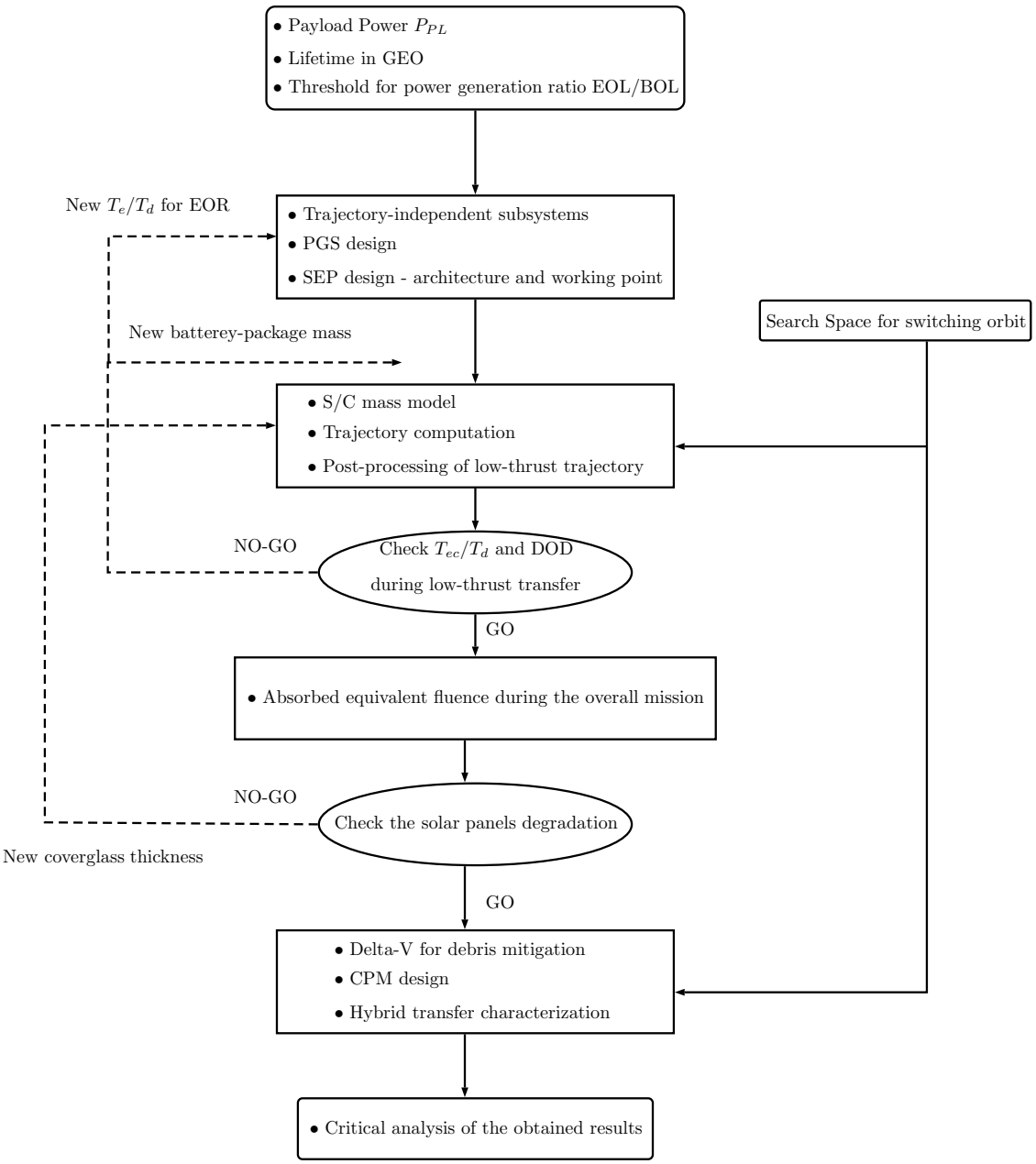

Fig. 12 Logical flow for Hybrid Transfer trajectory-system design.

CPM performances in Table 10, the initial mass for the low-thrust $m_{ep}\,(t_0)$, and the rocket equation, as Eq. (33) shows.

$$m_{\mathrm{pr,cp}} = \left(m_{\mathrm{CPM}} + m_{\mathrm{ep}}\,(t_0)\right) \tag{33}$$

In the end, the Hybrid Transfer mission to GEO is fully characterized in terms of injected mass in low-Earth orbit (LEO)

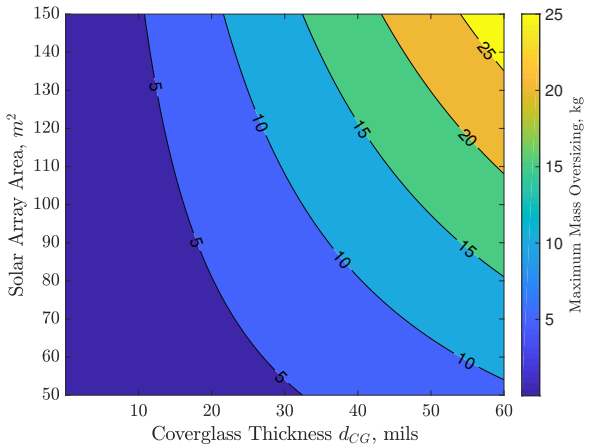

Fig. 13 Maximum burden mass due to the sizing procedure of coverglass thickness.

mass (Eq. (34)) and total time of flight (Eq. (35)).

$$m_{\text{LEO}} = m_{\text{pr,cp}} + m_{\text{CPM}} + m_{\text{ep}}\ (t_0) \tag{34}$$

$$\tau = \tau_{\text{cp,transfer}} + \tau_{\text{ep}} \tag{35}$$

VI. Parametric Analysis: numerical examples

The proposed system-trajectory optimization is presented in this section. The outcomes of the derived logical flow and the sensitivity of the mission performances to payload power variation are analyzed. The benefits of hybrid transfer approach will be assessed together with the effectiveness and robustness of the implemented backward strategy. Furthermore, as byproduct of this work-flow, low-thrust transfers to geostationary equatorial orbit (GEO) with various initial orbits are derived. This widens the trade space of solutions and enables us to shed light on the benefits of fully-electric propulsion (EP) spacecraft in combination with launcher's payload capability.

A. Case-Study

The investigation begins with a high payload power request of $P_{\text{pl}} = 20$ kW, with a corresponding payload mass m_{PL} = 1884 kg (obtained through Eq. (26)), an operative lifetime in GEO LF = 15 years, and a threshold degradation factor $L_{\text{d,min}} = P_{EOL}/P_{BOL} = 0.85\%$. Except for the fully-chemical transfer (FCT), which is characterized by a switching orbit that corresponds to GEO, the hybrid transfer (HT) solutions consider the Solar Electric Propulsion (SEP) configuration 2 (Fig. 10) with New Generation power processing unit (PPU) – BHT 8000 hall-effect thruster (HET).

The total available thrust is 1.014 N and the specific impulse is 1884 s for primary maneuvers. For orbit and attitude maintenance, the total available thrust and specific impulse are 0.268 N and 1916 s respectively. If the PPU requirements on the minimum voltage in Table 7 are relaxed, I_{sp} during electric orbit raising (EOR) decreases while

the thrust provided by SEP increases, thus lowering the time of flight. However, the consumed propellant increases marginally. The solar array area is 154.1 m^2 for each platform configuration since the power request at the GEO phase, which does not change whatever the HT path, is the primary factor that drives the SA sizing as outlined by Fig. 11. The parametric study is performed by initializing the grid of perigee and apogee radii selected for switching orbits, i.e., the ones in Fig. 2,

Figure 14a shows the injected mass in low-Earth orbit (LEO) (Eq. (34)) and the corresponding total transfer time τ (Eq. (35)). The isolines for τ display that different switching orbit entail different configurations of the platform since there is a variation in the encountered radiation environment and the bi-impulsive ΔV cost. The payload-customized mission design is illustrated in Fig. 14b, where the mass delivered to the final orbit is not constant (Eq. (3)) due to the differing EP phase performances, but it is bounded within the range of 4000–4550 kg. The SEP initial thrust-to-mass ratio is represented in Fig. 14c. Its variation meets the actual technology requirements for EP control authority of $10^{-4} - 10^{-3}$ m/s^2, and it plays a key role in tailoring the mass-at-target. As expected, the isolines for the EP transfer time in Fig. 14c suggest that τ_{ep} contributes the most to the total transfer time.

Low-Thrust Trajectory Optimisation (LT2O) solved 128 over 162 low-thrust minimum time transfers to GEO using the backward integration approach, the majority of which are in the region where the switching orbit eccentricity is lower than 0.4. The two point boundary value problem (TPBVP) is *soft-constrained* since some terminal quantities are fixed. For these time-optimal solutions, the maximum deviation between the computed final mass and the assumed one is 10.5 kg, i.e., the error between the obtained final mass and the one modeled through Eq. (3) is lower than 0.5 % of the minimum mass delivered into the Geostationary orbit.

The remaining 34 orbits are handled using the forward integration described in Work-flow 1. The median values of the relative error between final state and the GEO boundary conditions (e.g., position, velocity and inclination) are significantly low, i.e., 0.2751% and 0.2153% for position and velocity while 0.00097 deg for inclination. This behavior does not change qualitatively the outcomes of the proposed methodology, even if those paths are not time-optimized and they do not deliver exactly the payload in GEO.

The quantities related to eclipse encountered during the EP transfer are illustrated in Fig. 15. For sake of clarity, each result in that figure is the result of the first GO/NO-GO check of the logical flow shown in Fig. 12. The majority of HT platforms do not need to be equipped with extra energy source to manage the power request during the EP path. Fig. 15a shows the limits of the rechargeable battery package. The minimum is 235 kg and the maximum is 285 kg (only when the starting orbit apogee and perigee are towards the top left corner). The majority of the hybrid transfers entail only 235 kg of battery. The GEO platforms are nominally sized to contain batteries of that size (even without thruster operations during eclipses). Thus, in this case, using the existing battery package to assist the transfer, i.e, continuously thrusting and not pausing, would not have any major effect on the platform design. Similarly, the depth of discharge (DOD) value is illustrated in Fig. 15b: if it does not meet the mission requirements, battery cell shall be added

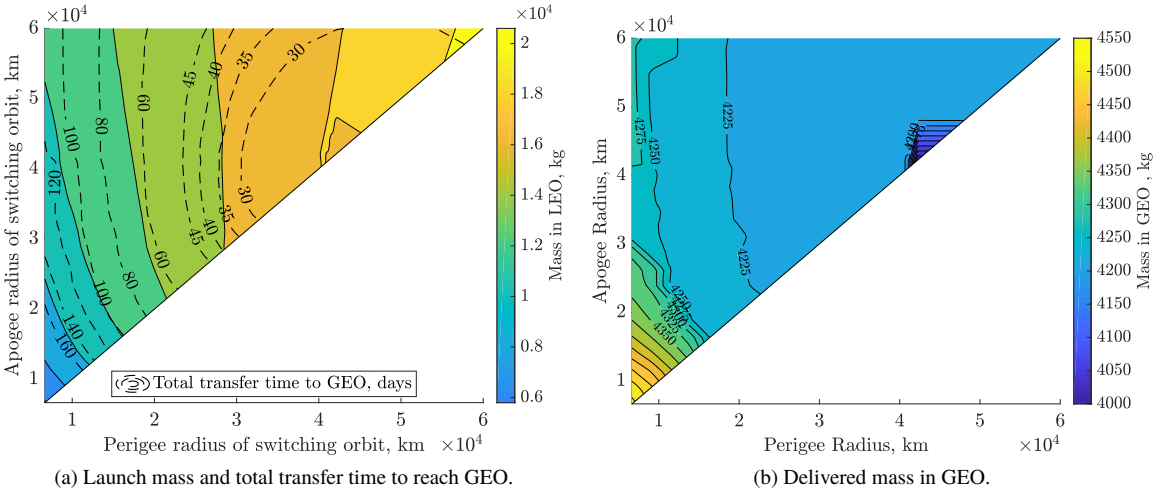

(a) Launch mass and total transfer time to reach GEO.

(b) Delivered mass in GEO.

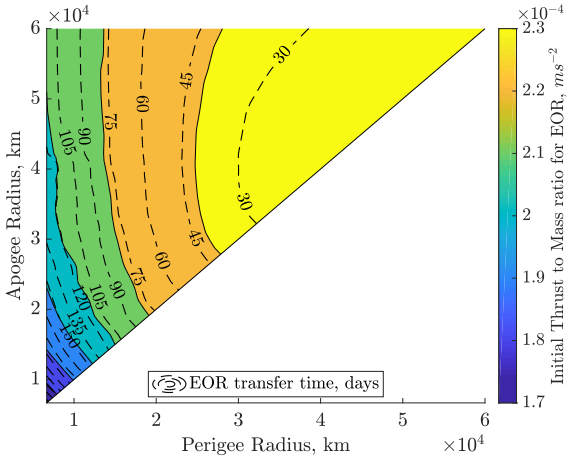

(c) Initial thrust-to-mass ratio and transfer time for EP phase.

Fig. 14 Features of hybrid transfer mission for 20 kW payload.

as described in Sec. IV.C. The maximum Earth-shadow period encountered during the transfer GEO is illustrated in Fig. 15c. An addition of an energy source enables continued payload operations and EP thruster operations even during eclipses in EOR phase, provided there is a feasible EP working point.

For all hybrid transfer solutions, the power generation ratio P_{EOL} / P_{BOL} does not exceed the set minimum value $L_{\mathrm{d,min}}$, as represented in Fig. 16a. Consequently, the trend of the absorbed total equivalent fluence at 1 MeVof electron behaves in accordance with the one of L_{d} as illustrated in Fig. 4, Sec. III.B. The higher the absorbed equivalent fluence, the lower the thickness. Referring to in Fig. 16b, $\Phi_{1MeV,\mathrm{TOT}}$ is higher for the switching orbits characterized by a perigee lower than medium Earth orbit (MEO) region and an apogee far from GEO. This result is interpreted by looking at Eqs. (22) to (24), together with Fig. 16c that illustrates the thickness of coverglass to shield the solar panels. Since the transfer is longer for orbits placed into the bottom left corner of the search grid, where the trapped particle with high energy are present, the coverglass thickness is increased to fulfill the constraint on $L_{\mathrm{d,min}}$. The maximum value of d_{cg} is

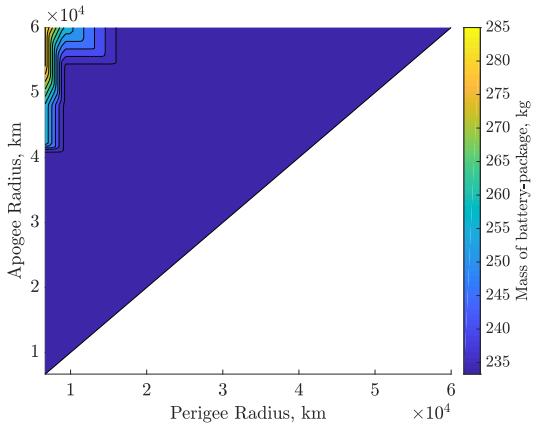

(a) Mass of rechargeable battery-package.

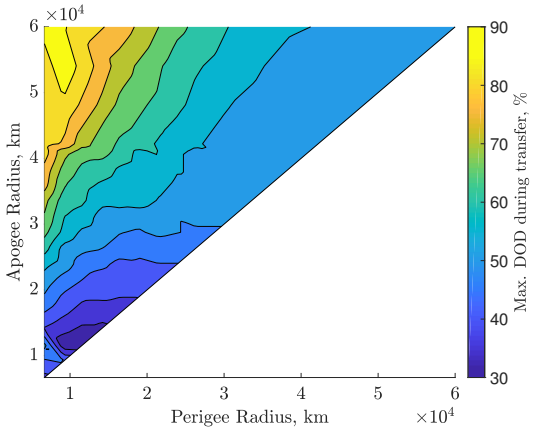

(b) Maximum DOD for low-thrust phase.

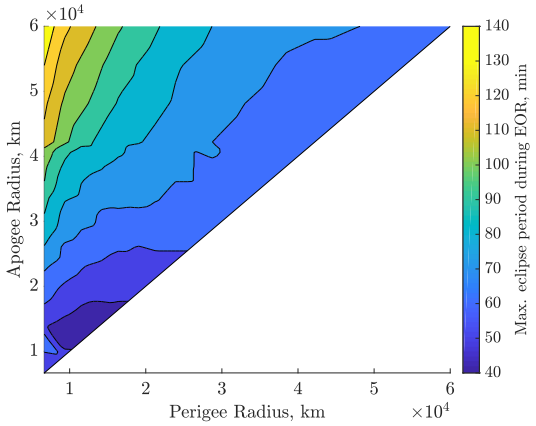

(c) Maximum eclipse duration for low-thrust phase.

Fig. 15 Results of eclipses for low-thrust phase.

~19.2 mils. Thus, if an increase in mass of ~ 192 kg can be tolerated, a standard value for the coverglass thickness can be used for all simulations.

Figure 17 outlines the main results of the chemical propulsion segment analysis. The total cost of the bi-impulsive maneuver (Fig. 17a), which includes chemical propulsion (CP) ΔV for debris mitigation (Eq. (15)), primarily affects the dry mass of the chemical module, as outlined in Fig. 17b.

Once the hybrid transfers to GEO missions are fully identified, the best injected mass versus transfer solutions are selected using the Pareto Optimality Criterion [56]. These family of solutions are outlined in Fig. 18a, where the FCT are fully-electric transfer (FET) can be observed as the boundaries for the set of the best HT. The Pareto-efficient solutions do not exceed the assumed LEO payload capacity for the selected launcher, i.e., 21000 kg (Sec. II.D). Furthermore, those solutions are analyzed and represented in terms of perigee and apogee radii of switching orbits in Fig. 18b.

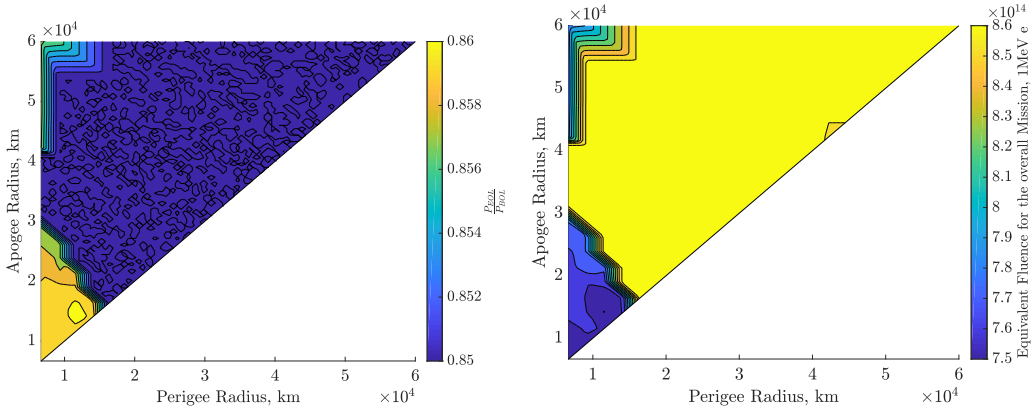

(a) Power EOL/BOL, referred to Eq. (22) .

(b) Cumulative $\Phi_{1\text{MeVe,TOT}}$, referred to Eq. (25).

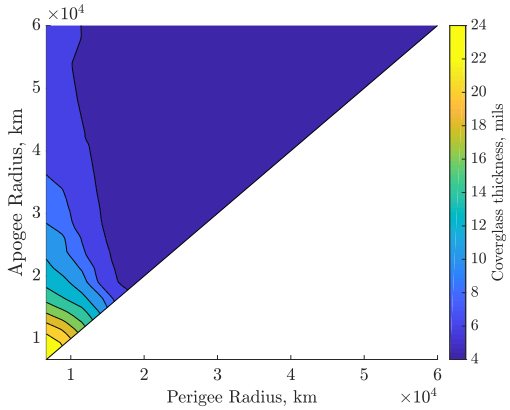

(c) Coverglass thickness for $L_d <= L_{\text{d,min}}$.

Fig. 16 Results of radiation analysis.

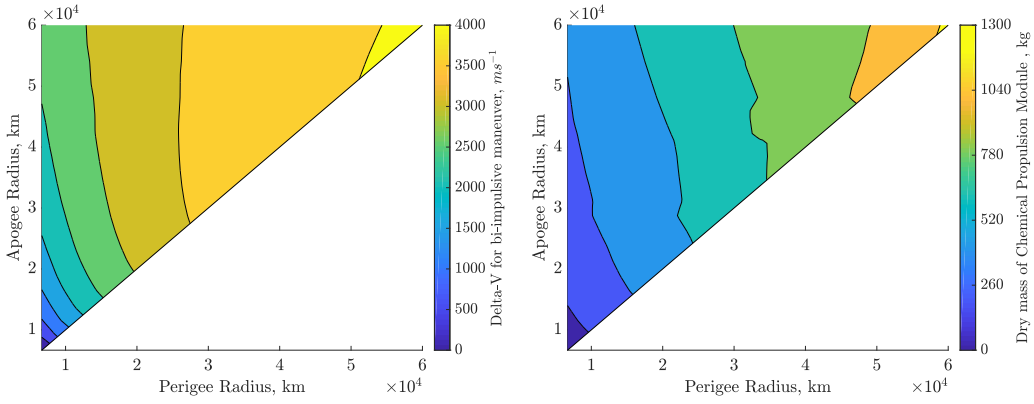

(a) Cost for bi-impulsive maneuver, referring to Eq. (13).

(b) Chemical module mass, referring to Eq. (32)

Fig. 17 Results of chemical propulsion phase analysis.

B. Variation of requested payload power

In addition to P_{PL} 20 kW scenario, the methodology proposed in Fig. 12 is applied to payload power requests of 10 kW and 15 kW. The other main input quantities are not varied, i.e., lifetime in GEO = 15 years and L_{dmin} = 0.85%.

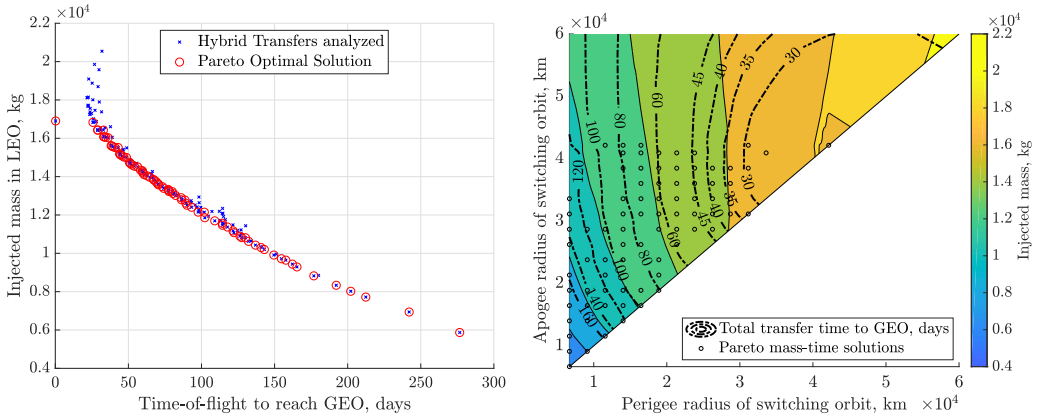

(a) Injected mass versus time

(b) Pareto Efficient solutions within the search grid framework.

Fig. 18 Pareto efficiency solutions for a payload power request of 20 kW.

Figure 19 illustrates the behaviors of the Pareto-efficient fronts for different payload power requests. The solutions move towards the top-right with increasing P_{PL}, thereby entailing heavier injected masses in LEO and longer transfers to GEO. This result emphasizes how an increment of P_{pl} affects the mass budget at launch more than the EP capability to propel the spacecraft, even if the available power at thruster level increases.

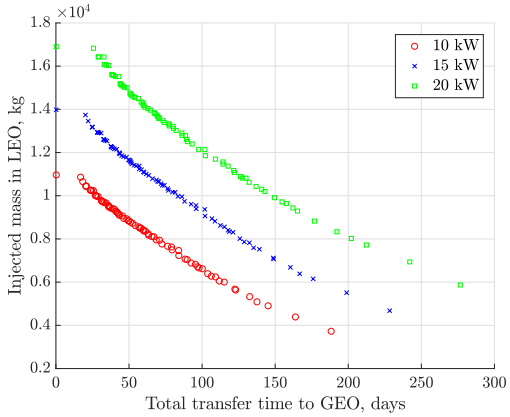

Fig. 19 Pareto-efficient solutions for payload power request of 10, 15, and 20 kW.

C. All-Electric Transfers to GEO

According to the payload capability model for Ariane 64 in Sec. II.D, Fig. 20 shows the combination of launch vehicle performances and all-electric transfer to GEO for the scenario described in Sec. VI.A. In general, the launch cost depends upon the launch vehicle, which has a tabulated cost per kg depending upon the injection orbit. The payload capacity of the launcher also depends upon the injection orbit. Focusing on the most representative injection space region to acquire the final orbit, i.e., perigee radius between 10000 and 25000 km and apogee between 10000 and 35000 km, the launcher's mass capacity over the initial mass of a single spacecraft for the EOR to GEO can be analyzed. One

may observe that several solutions allow launching more than one all-electric platform, which lead to decreasing the cost at launch since the launcher's costs could be shared between the spacecraft carried on by the launcher.

Fig. 20 illustrates the all-electric transfer solutions for GEO platform mass at launch for several injection orbits represented by a matrix of perigee and apogee radii. As the injection orbit semi-major axis increases, the platform mass decreases and the transfer time to GEO decreases. The launch vehicle (LV) payload capacity decreases with the increasing injection orbit semi-major axis. The ratio of the LV capacity and the platform mass is illustrated using dotted lines. For example, considering the initial injection orbit with perigee of 15000 km and apogee of 25000 km, the corresponding platform mass that utilizes an all-electric transfer is ~4500 kg. Ariane 6 payload capacity to that injection orbit is ~10000 kg. If the LV payload capacity for that particular injection orbit is 100% exploited, 2.2 platforms can be launched. This illustrates the customizable all-electric transfer solutions to GEO that are provided to the customers. Reduction in the initial mass and the accommodation of multiple platforms in a single launch leads to a decreased cost at launch.

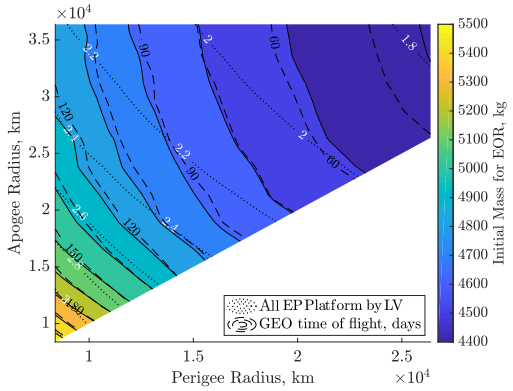

Fig. 20 FET to GEO for P_{pl} = 20 kW, LF = 15 y., and $L_{d_{min}}$ = 0.85 from several injection orbits superimposed on modeled Ariane 6 performances, referring to Eq. (18).

VII. Conclusion

The increasing trend in geostationary equatorial orbit (GEO) spacecraft signal throughput has led to an increase in power demand. Thus, GEO spacecraft are equipped with larger power systems and solar arrays, thereby increasing the mass. Traditional use of chemical propulsion, although providing a short transfer time, further increases the mass due to low specific impulse. Given the need to balance the mass and the time to commence service, a combined chemical–electric propulsion is proposed. The mission design of hybrid transfers to GEO with a prudent usage of chemical propulsion for high-thrust fast transfer phase and electric propulsion for low-thrust mass saving phase contributes towards achieving the objective of combined systems–trajectory design. Additionally, if the power spent during GEO operations and the electric orbit raising phases is balanced, the application of Solar Electric Propulsion also improves the satellite system design. The high amount of power intended to be supplied to the communication payload

during operations can be utilized to supply the electric propulsion (EP) during the low-thrust transfer phase. The higher the power, the higher is the EP thrust and specific impulse, which leads to a higher mass saving. However, practical limitations such as operations constraints during eclipses or spacecraft systems impact on the end of life performance should be investigated in more detail in future, which would advance the conceptual assessment.

The aim of this work was to create a novel combined systems–trajectory design solution, including radiation effects, for hybrid low-Earth orbit (LEO) to GEO transfers for GEO satellite platforms along. A systematic procedure is proposed to describe a new family of hybrid transfer solutions in pursuance to widen the trade space in designing GEO missions with high-power payload.

A wide set of solutions to reach GEO, where fully-chemical and fully-electric transfers represent the boundaries of the hybrid transfer trade space (Pareto-efficient transfers), is presented such that the customers can pick and choose the type of transfer and consequently the platform is characterized. The radiation absorption for each hybrid transfer (HT) solution is computed combining the latest AE9/AP9/SPM radiation models with solar protons events to give robustness to the overall analysis. The radiation damage of the solar cells is taken into account in the system-trajectory optimization design. Dual stage platform for HT is mass-efficient and time-of-flight efficient, but its design is complex to meet the requirements on mitigation of debris risk. A payload throughput power of 20 kW entails a spacecraft mass in GEO between 4000 kg and 4550 kg, an initial thrust-to-mass ratio range of $1.7 - 2.3 \times 10^{-4}$ m/s^2, and a coverglass thickness between 4 and 24 mils to guarantee a minimum end-of-life/beginning-of-life power ratio of 85%.

Considering the payload capability of new launchers such as Ariane 6, fully-electric transfer (FET) from injection orbits different than the classical geosynchronous transfer orbit (GTO) and super synchronous transfer orbit (SSTO) are proposed to widen the trade space in designing all-electric solutions to GEO. These solutions yield transfer to GEO with with time-of-flight from 60 to 150 days and a light initial mass for the platform, 4400–5500 kg.

Finally, as incentive for a future improvements, it is acknowledged that the placement of a satellite into GEO is a profitable but complex task. Therefore, the overall benefits of hybrid transfer shall be further evaluated by using economical models as well; for example, a detailed costs analysis needs to be performed for launchers, ejectable chemical propulsion module, and satellite systems.

Acknowledgments

This research was supported by Regione Lombardia and Fondazione Cariplo through the SpaceSHIP (Space Systems with Hybrid Propulsion) project, Grant No. AD15VARI04.

References

[1] Miele, A., and Wang, T., "Optimal Planetary Orbital Transfers via Chemical Engines and Electrical Engines," *Journal of Optimization Theory and Applications*, Vol. 127, No. 3, 2005, pp. 587–604. doi:10.1007/s10957-005-7505-x.

[2] del Amo, J. G., "Activities on Electric Propulsion at ESA," *5th Space Propulsion Conference, Rome, Italy*, 3AF - Association Aèronautique et Astronautique de France, 2016, pp. 1–10.

[3] "The Annual Compendium of Commercial Space Transportation: 2018", Federal Aviation Administration, United States, Jan 2018.

[4] Edelbaum, T. N., "The use of high and low-thrust propulsion in combination for space missions," *Journal of the Astronautical Sciences*, Vol. 9, No. 2, 1962, pp. 49–69. .

[5] Oleson, S. R., Myers, R. M., Kluever, C. A., Riehl, J. P., and Curran, F. M., "Advanced Propulsion for Geostationary Orbit Insertion and North-South Station Keeping," *Journal of Spacecraft and Rockets*, Vol. 34, No. 1, 1997, pp. 22–28. doi:10.2514/2.3187.

[6] Sackett, L. L., Malchow, H. L., and Edelbaum, T. N., "Solar Electric Geocentric Transfer With Attitude Constraints: Analysis," Tech. Rep. NASA CR-134927, NASA, United States, 1975.

[7] Mailhe, L. M., Heister, S. D., and Lafayette, W., "Design of a Hybrid Chemical / Electric Propulsion Orbital Transfer Vehicle," *Journal of Spacecraft and Rockets*, Vol. 39, No. 1, 2002, pp. 131–139. doi:10.2514/2.3791.

[8] Oh, D., Randolph, T., Kimbrel, S., and Martinez-Sanchez, M., "End-to-End Optimization of Chemical-Electric Orbit-Raising Missions," *Journal of Spacecraft and Rockets*, Vol. 41, No. 5, 2004, pp. 831–839. doi:10.2514/1.13096.

[9] Kluever, C. A., "Optimal Geostationary Orbit Transfers Using Onboard Chemical-Electric Propulsion," *Journal of Spacecraft and Rockets*, Vol. 49, No. 6, 2012, pp. 1174–1182. doi:10.2514/1.A32213.

[10] Kluever, C. A., "Designing Transfers to Geostationary Orbit Using Combined Chemical–Electric Propulsion," *Journal of Spacecraft and Rockets*, Vol. 52, No. 4, 2015, pp. 1144–1151. doi:10.2514/1.A33259.

[11] Kluever, C. A., "Optimal Earth-Moon Trajectories Using Combined Chemical-Electric Propulsion," *Journal of guidance, control, and dynamics*, Vol. 20, No. 2, 1997, pp. 253–258. doi:10.2514/2.4060.

[12] Topputo, F., Mingotti, G., and Bernelli-Zazzera, F., "Enhancing Planetary Exploration by Using Hybrid Propulsion Transfers," *63rd International Astronautical Congress (IAC), Naples, Italy*, 2012, pp. 5483–5491.

[13] Topputo, F., and Massari, M., "Modeling and Optimization of Hybrid Transfers to Near-Earth Objects," *Modeling and Optimization with Case Studies*, Springer, New York, G. Fasano and J. Pintèr Editors, 2017, pp. 425–442. doi:10.1007/978-3-319-41508-6_16.

[14] Mingotti, G., Topputo, F., and Massari, M., "Hybrid Propulsion Transfers for Mars Science Missions," *23rd AAS/AIAA Space Flight Mechanics Meeting, Kauai, Hawaii, United States*, 2013, p. AAS 13–385.

[15] Mani, K. V., Cervone, A., and Topputo, F., "Combined Chemical–Electric Propulsion for a Stand-Alone Mars CubeSat," *Journal of Spacecraft and Rockets*, 2019, pp. 1–15. doi:10.2514/1.A34519.

[16] Oberth, H., *Ways to spaceflight*, NASA-TFF-622, National Aeronautics and Space Administration, 1972.

[17] IADC Working Group 4, *Support to the IADC Space Debris Mitigation Guidelines*, Inter-Agency space Debris Coordination Committee, 2014.

[18] Vallado, D. A., *Fundamentals of Astrodynamics and Applications*, 4th ed., Microcosm Press and Springer, 2013, Chap. 6, pp. 351–354. ISBN: 9781881883197.

[19] Topputo, F., and Ceccherini, S., "A catalogue of parametric time-optimal transfers for all-electric GEO satellites," *In: Fasano G., Pintér J. (eds) Modeling and Optimization in Space Engineering*, Vol. 144, Springer, 2019, pp. 459–478. doi:10.1007/978-3-030-10501-3_17.

[20] Cefola, P. J., "Equinoctial orbit elements-Application to artificial satellite orbits." *Celestial Mechanics*, Vol. 5, 1972. doi: 10.2514/6.1972-937.

[21] La Mantia, M., and Casalino, L., "Indirect optimization of low-thrust capture trajectories," *Journal of Guidance Control and Dynamics*, Vol. 29, No. 4, 2006, pp. 1011–1014. doi:10.2514/1.18986.

[22] Randolph, T., and Oh, D., "Economic Benefit Analysis of Chemical-Electric Orbit Raising Missions," *20th AIAA International Communication Satellite Systems Conference and Exhibit, Montreal, Canada*, AIAA, 2002, pp. AIAA–02–1980.

[23] Hofer, R., Randolph, T., Oh, D., Snyder, J., and de Grys, K., "Evaluation of a 4.5 kW Commercial Hall Thruster System for NASA Science Missions," *42nd AIAA - American Society of Mechanical Engineers - Society of Automotive Engineers - American Society for Engineering Education Joint Propulsion Conference & Exhibit, Sacramento, California, United States*, AIAA, 2006, p. 4469. doi:10.2514/6.2006-4469.

[24] Topputo, F., and Bernelli-Zazzera, F., "Optimal Low-Thrust Stationkeeping of Geostationary Satellites," *CEAS Conference Proceedings, Perth, Australia*, 2011, pp. 1917–1925.

[25] Haberkorn, T., Martinon, P., and Gergaud, J., "Low Thrust Minimum-Fuel Orbital Transfer: A Homotopic Approach," *Journal of Guidance, Control, and Dynamics*, Vol. 27, No. 6, 2004, pp. 1046–1060. doi:10.2514/1.4022.

[26] Graham, K. F., and Rao, A. V., "Minimum-Time Trajectory Optimization of Multiple Revolution Low-Thrust Earth-Orbit Transfers," *Journal of Spacecraft and Rockets*, Vol. 52, No. 3, 2015, pp. 711–727. doi:10.2514/1.A33187.

[27] Lagier, R., "Ariane 5 User's Manual", Issue 5 Revision 2 Arianespace, October 2016.

[28] "Semi-analytic Tool for End of Life Analysis (STELA) User's Guide", CNES, December 2019.

[29] Lagier, R., "Ariane 6 User's Manual", Issue 1 Rev. 0, Arianespace, 2018.

[30] Ginet, G. P., O'Brien, T. P., Huston, S. L., Johnston, W. R., Guild, T. B., Friedel, R., Lindstrom, C. D., Roth, C. J., Whelan, P., Quinn, R. A., Madden, D., Morley, S., and Su, Y.-J., "AE9, AP9 and SPM: New Models for Specifying the Trapped Energetic Particle and Space Plasma Environment," *Space Science Reviews*, Vol. 179, No. 1, 2013, pp. 579–615. doi:10.1007/s11214-013-9964-y.

[31] Messenger, S. R., Wong, F., Hoang, B., Cress, C. D., Walters, R. J., Kluever, C. A., and Jones, G., "Low-Thrust Geostationary Transfer Orbit (LT2GEO) Radiation Environment and Associated Solar Array Degradation Modeling and Ground Testing," *IEEE Transactions on Nuclear Science*, Vol. 61, No. 6, 2014, pp. 3348–3355. doi:10.1109/TNS.2014.2364894.

[32] Kruglanski, M., Messios, N., De Donder, E., Gamby, E., Calders, S., Hetey, L., and Evans, H., "Space environment information system (SPENVIS)," *EGU General Assembly Conference Abstracts, Vienna, Austria*, 2009, p. 7457.

[33] Xapsos, M. A., Summers, G. P., Barth, J. L., Stassinopoulos, E. G., and Burke, E. A., "Probability model for cumulative solar proton event fluences," *IEEE Transactions on Nuclear Science*, Vol. 47, No. 3, 2000, pp. 486–490. doi:10.1109/23.856469.

[34] "NeXt Triple Junction (XTJ) Solar Cells", Spectrolab, September 2012.

[35] Tada, H. Y., Carter Jr, J. R., Anspaugh, B. E., and Downing, R. G., *Solar cell radiation handbook*, National Aeronautics and Space Administration, 1982, Chap. 3, pp. 3–1 — 3–58.

[36] Anspaugh, B. E., and Downing, R. G., "Radiation effects in silicon and gallium arsenide solar cells using isotropic and normally incident radiation," Tech. rep., NASA, United States, 1984.

[37] Messenger, S. R., Summers, G. P., Burke, E. A., Walters, R. J., and Xapsos, M. A., "Modeling solar cell degradation in space: A comparison of the NRL displacement damage dose and the JPL equivalent fluence approaches," *Progress in Photovoltaics: Research and Applications*, Vol. 9, No. 2, 2001, pp. 103–121. doi:10.1002/pip.357.

[38] Fetzer, C., Jun, B., Edmondson, K., Khemthong, S., Rouhani, K., Cravens, R., Bardfield, R., and Gillanders, M., "Production ready 30% efficient triple junction space solar cells," *33rd IEEE Photovoltaic Specialists Conference, San Diego, United States*, 2008, pp. 1–4.

[39] Yudintsev, A. G., "Energy conversion complexes for ground testing of spacecraft power supply systems (in Russian)," *Proceedings of Tomsk State University of Control Systems and Radioelectronics*, Vol. 22, No. 3, 2019, pp. 95–102.

[40] Fenech, H., Sonya, A., Tomatis, A., Soumpholphakdy, V., and Serrano Merino, J. L., "Eutelsat quantum: a game changer," *33rd AIAA International Communications Satellite Systems Conference and Exhibition, Queensland, Australia*, 2015, p. 4318.

[41] Klaus, K. K., Elsperman, M., and Rogers, F., "Mission Concepts Enabled by Solar Electric Propulsion and Advanced Modular Power Systems," *AAS/Division for Planetary Sciences Meeting Abstracts# 45, Denver, Colorado, United States*, 2013, pp. 211–14.

[42] Kodys, A., Pilchuk, J., Glogowski, M., Trescott, J., Pucci, J., and Koch, B., "Initial Flight Operations of the GEOStar-3 Electric Propulsion System," *2018 AIAA - American Society of Mechanical Engineers - Society of Automotive Engineers - American Society for Engineering Education Join Propulsion Conference, Cincinnati, Ohio, United States*, 2018, p. 4719.

[43] Peukert, M., and Wollenhaupt, B., "OHB-System's view on electric propulsion needs," *EPIC Workshop, Brussels, Belgium*, 2014, pp. 1–48.

[44] Mauroschat, A., Lascar, S., Cussac, T., Roux, M., and Patier, M., "Alphabus: Europe's solution for the high-power satcom market", European Space Agency (ESA) Bulletin 142, May 2010.

[45] Wertz, J. R., Everett, D. F., and Puschell, J. J., *Space Mission Engineering: the New SMAD*, Microcosm Press, 2011, Chaps. 18,21, App.A, pp. 541–552, 641–662, 941–954. ISBN: 9781881883159.

[46] Goebel, D. M., and Katz, I., *Fundamentals of electric propulsion: Ion and Hall thrusters*, John Wiley & Sons, 2008. ISBN: 978-0470436448.

[47] Rovey, J. L., Lyne, C. T., Mundahl, A. J., Rasmont, N., Glascock, M. S., Wainwright, M. J., and Berg, S. P., "Review of multimode space propulsion," *Progress in Aerospace Sciences*, Vol. 118, 2020, p. 100627. Doi: 10.1016/j.paerosci.2020.100627.

[48] Szabo, J., Pote, B., Byrne, L., Paintal, S., Hruby, V., Tedrake, R., Kolencik, G., Freeman, C., and Gatsonis, N., "Eight Kilowatt Hall thruster system characterization," *33rd International Electric Propulsion Conference, Washington, D.C., United States*, 2013, pp. 1–8.

[49] Duchemin, O., Dumazert, P., Cornu, N., Estublier, D., and Darnon, F., "Stretching the operational envelope of the PPS ®X000 plasma thruster," *40th AIAA - American Society of Mechanical Engineers - Society of Automotive Engineers - American Society for Engineering Education Join Propulsion Conference, Fort Lauderdale, Florida, United States*, 2004, p. 3605. doi:10.2514/6.2004-3605.

[50] Topputo, F., Long, R., Mingotti, G., and Massari, M., "Hybrid Propulsion Transfer Strategies," Tech. Rep. 105465/12/NL/AF, ESA/ESTEC, 2012.

[51] Duchemin, O., Leroi, V., Vial, V., Öberg, M., Bourguignon, É., Scalais, T., Demairé, A., and Lübberstedt, H., "Electric propulsion thruster assembly for Small GEO," *46th AIAA - American Society of Mechanical Engineers - Society of Automotive Engineers - American Society for Engineering Education Joint Propulsion Conference & Exhibit, Nashville, Tennessee, United States*, 2010, p. 6696.

[52] Bourguignon, E., and Fraselle, S., "PPU MK3 For 5 KW Hall Effect Thrusters," *11th European Space Power Conference - E3S Web of Conferences, Juan-les-Pins, Côte d'Azur, France,*, Vol. 16, EDP Sciences, 2017, p. 15001. doi:10.1051/e3sconf/20171615001.

[53] "BHT-200 Busek Hall Effect Thruster", Busek Inc., December 2019.

[54] "Power System Regulator (PSR) 100V - A single integrated & modular unit to power your Satcom between 8kW and 23kW", Airbus Defence and Space SAS, 2019.

[55] "LSE51 - Lithium Ion Cells For Satellites–Power Optimized", GS Yuasa Lithium Power, 2017. URL `http://www.gsyuasa-lp.com/SpecSheets/GS_Yuasa_LSE_GEN_III_Power.pdf`.

[56] Luc, D. T., Chinchuluun, A., Pardalos, P. M., Migdalas, A., and Pitsoulis, L., *Pareto Optimality*, Springer New York, New York, NY, 2008, Chap. Part 2, pp. 481–515. doi:10.1007/978-0-387-77247-9_18.